1-1-2016

Design and Control of Islanded Microgrid

Zeya Cai
University of Denver

Design and Control of Islanded Microgrid

Abstract

The control of frequency and power has always been a problem in the development of microgrid. This thesis focuses on the design and control of islanded microgrid; more specifically, it includes the design of the PV system and wind power system and the control of the frequency, voltage and the power output of the islanded microgrid.

Microgrid consists of the power sources, the control system, the distribution network and the load. More specifically, the power sources are composed of PV system and wind turbine system; the control system in the microgrid includes the droop controller, the Maximum Power Point Tracking (MPPT) controller and the pitch controller.

This thesis is dedicated to researching the control of the islanded microgrid. The frequency and the power output in islanded microgrid can be controlled by using different kinds of controllers. Since PV and wind turbine have different structures and characteristics, the control systems for the PV and wind turbine are different. It is also necessary to let the PV system and the wind power system communicate with each other in order to control the total power output to the load.

The design of the islanded microgrid includes the design of the PV system and design of the wind power system. This thesis includes five chapters. The first chapter includes the introduction to the microgrid, some background and motivation, literature review and the expected contributions. Then the thesis describes the PV system and the wind power system in chapter 2 and chapter 3 respectively. In both chapter 2 and chapter 3, the general structure of each system is shown first and then the details of the systems are discussed. The control system includes the controllers such as the MPPT controller, the pitch controller and the droop controller. A modified controller is introduced in chapter 2, which is the droop controller integrated with virtual inertia. A testing case comparing the frequency control with the modified droop controller and the droop controller is also shown in the same chapter.

The fourth chapter tests the control system of the microgrid by showing five testing cases and comparing two different experimental sets (load 1 and load 2); the last chapter concludes the thesis and discusses the future work of the design.

Document Type

Thesis

Degree Name

M.S.

Department

Electrical Engineering

First Advisor

David Wenzhong Gao, Ph.D.

Second Advisor

Andrew Detzel, Ph.D.

Third Advisor

Amin Khodaei

Keywords
Islanded microgrid, Maximum power point tracking, MPPT, Wind power

Subject Categories
Electrical and Computer Engineering

Design and Control of Islanded Microgrid

_____

A Thesis

Presented to

the Faculty of the Daniel Felix Ritchie School of Engineering and Computer Science

University of Denver

_____

In Partial Fulfillment

of the Requirements for the Degree

Master of Science

_____

by

Zeya Cai

November 2016

Advisor: Dr. David Wenzhong Gao

Author: Zeya Cai
Title: Design and Control of Islanded Microgrid
Advisor: Dr. David Wenzhong Gao
Degree Date: November 2016

Abstract

The control of frequency and power has always been a problem in the development of microgrid. This thesis focuses on the design and control of islanded microgrid; more specifically, it includes the design of the PV system and wind power system and the control of the frequency, voltage and the power output of the islanded microgrid.

Microgrid consists of the power sources, the control system, the distribution network and the load. More specifically, the power sources are composed of PV system and wind turbine system; the control system in the microgrid includes the droop controller, the Maximum Power Point Tracking (MPPT) controller and the pitch controller.

This thesis is dedicated to researching the control of the islanded microgrid. The frequency and the power output in islanded microgrid can be controlled by using different kinds of controllers. Since PV and wind turbine have different structures and characteristics, the control systems for the PV and wind turbine are different. It is also necessary to let the PV system and the wind power system communicate with each other in order to control the total power output to the load.

The design of the islanded microgrid includes the design of the PV system and design of the wind power system. This thesis includes five chapters. The first chapter includes the introduction to the microgrid, some background and motivation, literature

review and the expected contributions. Then the thesis describes the PV system and the wind power system in chapter 2 and chapter 3 respectively. In both chapter 2 and chapter 3, the general structure of each system is shown first and then the details of the systems are discussed. The control system includes the controllers such as the MPPT controller, the pitch controller and the droop controller. A modified controller is introduced in chapter 2, which is the droop controller integrated with virtual inertia. A testing case comparing the frequency control with the modified droop controller and the droop controller is also shown in the same chapter.

The fourth chapter tests the control system of the microgrid by showing five testing cases and comparing two different experimental sets (load 1 and load 2); the last chapter concludes the thesis and discusses the future work of the design.

Acknowledgements

First of all, I would like to express my highest gratitude to my professor and advisor David Wenzhong Gao for his tremendous support and encouragement during my two years of study at University of Denver. In my graduate study, he teaches me how to read paper efficiently and how to write good thesis. What is more, professor Gao's earnest attitude towards knowledge and his selfless contribution to students makes me believe that an excellent professor not only pays attention to the research, but also teaches student how to contribute to the world and makes the society better.

I am also very grateful to the committee members: professor Jason Jun Zhang, professor Amin Khodaei and professor Andrew Detzel. I fully appreciate your time in coming to my oral defense and giving your valuable suggestions.

Meanwhile, I cannot hide my gratitude to my lab partners such as Weihang Yan, Xiao Wang and Qiao Li. Their tons of advice and countless help make me finish this thesis.

Last but not the least, I really appreciate my family for their everlasting love and support.

Table of Contents

List of Figures

Chapter One: Introduction

1.1 Background and Motivation

It is universally acknowledged that the control of power has been a crucial problem in microgrid. In microgrid, the control of active power, reactive power, voltage, frequency are all challenges. Even a small mistake in control of power could cause severe damage to the whole power system; for instance, the Northeast Blackout which had caused millions of people away from the electricity throughout parts of the Northeastern and Midwestern United States and the Canadian province of Ontario, happened because of the control problem of the alarm system. A lack of alarm left operators unaware of the need to re-distribute power after overloaded transmission lines hit unpruned foliage, which triggered a race condition in the control software [1]. Another instance is the 2012 India Blackout, in which two severe power blackouts caused a shortage of 32 GW and affected over 300 million people on 30 and 31 July 2012 [2]. The problem of power outages has made many disasters and tragedies in human history, and most of them happened due to the poor control of the power grid. Therefore, it is crucial to make sure that power is running under good control.

Furthermore, the environment has been affected by the traditional power generation methods. However, microgrid is capable of integrating renewable resources such as wind and solar, which has much less pollution than that of the traditional power

sources. As an environmentalist who is interested in power and energy, I am determined to focusing on the design and control of the microgrid.

1.2 Definition

There are a number of definitions for microgrid. The U.S. Department of Energy defines microgrid as "a bunch of interconnected loads and distributed energy resources with boundaries that performs as an entity with control capability". The Working Group, Microgrid Evolution Roadmap describes it as an "electricity distribution system that consists of distributed generators and loads that can be operated coordinately either while connected to the power grid or while isolated" [3]. From the definition of EU research projects, microgrid is composed of low-voltage distribution systems with distributed energy resources (PV, wind turbine and fuel cell) and storage devices such as energy storage system and flywheels [4]. The primary purpose is to ensure local, reliable, and affordable energy security for urban and rural communities. It also provides solutions for commercial, industrial, and federal government consumers [5]. Furthermore, microgrid can be connected and disconnected from the grid to enable it to operate in either grid-connected or islanded mode. An ideal microgrid should also perform the following benefits as shown below [6]:

- "Ensures power quality, reliability, and security for end users and operators of the grid"
- "Elevates the integration level of distributed and renewable energy resources"
- "Cost competitive and efficient"

- “Enables smart grid technology integration”
- “Minimize carbon footprint and green house gas emissions by maximizing clean local energy generation”

1.3 Literature Review

There are various kinds of microgrids which consist of different distributed generators and different components. Paper [7] builds the microgrid by combining the generators such as photovoltaic array and fuel cell stack with power electronic interfacing circuits including boost converter and PWM inverter. Paper [8] integrates the renewable energy resources and energy storages system to build a microgrid. The main advantage of the microgrid is that it can supply power when the power outage occurs by switching between islanded mode and grid-connected mode [9].

There are also many kinds of methods of controlling the microgrid. According to different functions of distributed generators, the control mode of microgrid control can be categorized into master-slave control mode, peer-to-peer control mode and hierarchical control mode.

1.3.1 Master-Slave Control

Master-slave control system usually consists of a leading power supply and multiple following power resources. The leading power supply adopts the nominal voltage, frequency and control mode, which has the output characteristic of the voltage source and has large capacity. When the microgrid is operating in islanded mode, it replaces the main grid to provide the necessary inertia response for the frequency and voltage stability. The power supply with constant control and current source output

characteristics can make sure that distributed generators work at the maximum power point; furthermore, multiple distributed generators can be connected in parallel to expand power generation capacity. However, the application of this method is very limited because the redundancy and reliability of the master-slave control system cannot be guaranteed. It is mainly applicable to the system with large main power supply capacity, sufficient margin and islanded power supply demand. It is also useful for the system that rarely works in islanded mode of operation of the microgrid [10].

1.3.2 Peer-to-peer control

Compared with the master-slave control, the peer-to-peer control mode can greatly improve the redundancy of the system and implement the "plug and play" function of the generators. Because all the distributed generators in the microgrid have the same status, there is no master-slave relationship among the distributed generators and each distributed generator detects the voltage and frequency of microgrid based on the local condition.

Droop control method is one of the most popular peer-to-peer control modes [11], which has the advantages including: 1) microgrid can be connected and disconnected from the power grid with seamless switching [12]; 2) each distributed generator can provide a certain voltage and frequency support when disconnected from the power grid; 3) distributed generators equipped with droop controller can automatically participate in the power output distribution and easy to achieve "plug and play", which saves the cost of the communication system. Droop control is implemented by simulating the droop characteristic of the traditional synchronous generator in the power electronic interface of the distributed generators so that the active power output of the distributed generators is

increased when the system frequency is reduced; when the voltage of the generators decreases, the reactive power output of the distributed generators is increased. Thus, when the microgrid runs in islanded mode, each distributed generators with droop control can participate in the regulation of voltage and frequency of the microgrid. When the load changes, the load is automatically divided according to the droop coefficient and therefore achieving the rational distribution of the output power of generators and the microgrid can re-achieve a stable working condition. Figure 1.1 shows the block diagram of the droop control system.

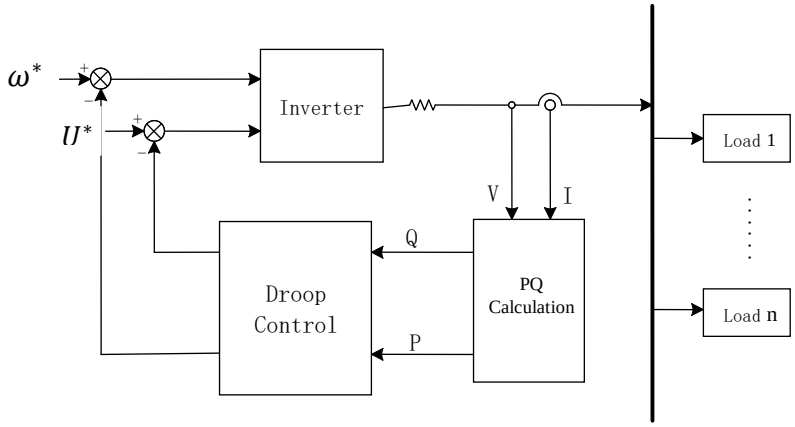

Fig.1.1 Diagram of Droop control

At present, most of the microgrid systems with droop control still remain in the experimental stage. How to improve the stability of microgrid system with droop control is still a problem that many researchers are trying to solve.

1.3.3 Hierarchical Control

Although droop controller can realize automatic power allocation and wireless interconnection between the distributed generators, excessive load fluctuation will still cause large deviation of frequency and voltage in the microgrid. Therefore, on the basis

of droop control, literature [13] proposed an hierarchical control structure for DC microgrid and inverter AC microgrid. The hierarchical control structure divides the microgrid control system into three levels: 1) A primary control includes droop controller and voltage-current controller that is capable of allocating power automatically; 2) Droop control (Secondary Control) that is based on the deviation of voltage and frequency; 3) Tertiary control that manages the energy dispatching in the microgrid or between the microgrid and the distribution network to achieve optimal scheduling of the microgrid.

In the hierarchical control structure, the primary control belongs to the local controller of distributed generators, while the secondary control and the tertiary control belong to the microgrid centralized control. However, with the development of distributed cooperative control technology and multi-agent cooperative control technology, the secondary controller of microgrid tends to be distributed among distributed generators [14]. Decentralized secondary control is more conducive to improving the reliability of microgrid control system and the "plug and play" capability of distributed generators.

1.3.4 Inverter-based microgrid

At present, the research of power conversion technology is relatively mature for the distributed power generation units and power electronic interfaces. The mathematical model of photovoltaic cells and PV inverters are established in paper [15]. In this paper, the maximum power point tracking problem of PV inverters is solved by the Extreme Seeking Algorithm. Literature [16] describes a simplified model of doubly-fed induction generator for wind power generation system. The application of flywheel energy storage

system (ESS) in microgrid is described in literature [17]. The application of energy storage system with battery and super capacitor is discussed in paper [18].

As mentioned above, the modeling and control of the power electronics interface and power conversion technology in various generators are relatively mature. On the other hand, the control strategy design for the whole microgrid system model is still inadequate, especially for inverter-type AC microgrid in the islanded operation mode. However, there are still many experts and scholars who have made great contributions to this topic. For example, paper [19] uses the local primary control structure of the AC microgrid of the inverter. First, the linear model of each distributed generator at the equilibrium point is obtained by means of small-signal linearization. Then, the linearization model of microgrid system is formed by integrating the generators system through coordinate transformation. In addition, the detailed simulation results show that the local primary control structure can maintain the stable operation of microgrid when the load disturbance of each distributed generator is less than 1/3 of its output capacity. This paper has made outstanding contributions to the study of microgrid stability. In paper [20], the author integrated the PV panel, the MPPT, the DC bus and the inverter in the integrated modeling and controller design. In paper [21], the dynamic modeling and control of the AC / AC hybrid microgrid with wind power generation units are studied.

1.3.5 Impact of high renewable energy penetration on microgrid systems

On the one hand, microgrid provides an effective way to access the grid for a variety of distributed generators. On the other hand, microgrid plays an important role in improving the reliability of the power supply and this solves the problem of power supply

in many remote areas, which enables the local power grid operate when disconnected from the main power grid and thus reducing power loss in the long-distance transmission. Although the application of microgrid has a lot of advantages, there are still many crucial technical issues to be resolved.

In the traditional power grid, the rotating rotor contains the moment of inertia when the large-scale synchronous generator is running; so the synchronous generator can release the kinetic energy contained in the rotor rapidly when the grid load suddenly increases or the power output of one generator drops. It also transfers kinetic energy into active power output in order to reduce the drop of frequency [22]. However, for the microgrid with distributed generators, the power electronic transformations (inverters) in distributed generator systems do not have the same rotational inertia as traditional synchronous generators. As the grid generation system is required to work at the maximum power point [23], the distributed generators cannot provide the inertia response to the grid when the load changes. Therefore, the penetration of the high renewable energy microgrid will greatly affect the power quality of power systems. For the wind power generation system, although the inertia exists in the wind turbine, it must use the power electronic converter to connect the AC microgrid to ensure the output power frequency is synchronized with the power grid so the inertia is isolated by the power electronic converter from the microgrid. Ideally, we expect as many new sources (PV, wind power) of distributed energy resources as possible to increase the penetration of new energy in the grid; at the same time, distributed generators of new energy are replacing the traditional synchronous generators. In the microgrid, penetration and low

inertia of new energy will inevitably cause large disturbances in the transient instability, which is discussed in the literature [24][25][26].

At present, the main method to solve the low inertia problem in microgrid is to limit the maximum output power of distributed generator and to advance the maximum power point tracking algorithm (MPPT) to ensure the existence of output margin of distributed generators that use new energy as resources. The reserved output margin emulates the inertia of synchronous generators in conventional power grid and provides support for microgrid system. However, this method results in low efficiency of new energy power generation and there is a great deal of randomness due to the environmental impact. Take the photovoltaic power generation system and wind power system as examples, the distributed generators still cannot provide the inertia to the microgrid with low irradiance and low wind. In response to the randomness of the new energy generators output, there are many experts and scholars using ESS to provide a certain inertia corresponding for the microgrid [27]. The ESS can be mixed with the DGs such as the PV system and the wind power system, which makes distributed generators output power smoothly and provide inertia to the microgrid. Meanwhile, the ESS can be directly embedded in the microgrid bus and provide inertia support to the microgrid directly. The capacity of the ESS directly embedded in the microgrid bus is required to be large enough to supply power to the microgrid when the distributed generators do not supply power or get charged when there is excess power from the distributed generators.

This thesis focuses on the islanded operation mode of the microgrid. In terms of the PV system, the Maximum Power Point Tracking (MPPT) controller and the droop controller are essential. In terms of the wind power system, the MPPT control and the

pitch controller are necessary. In the PV system, the droop control based on virtual inertia is designed, which has better control capability to improve frequency stability. The details are discusses in chapter 2.

1.4 Expected Contribution

This thesis intends to focus on the design and especially the control of the microgrid. Basically, the testing results should prove that this thesis has the expected contribution in the following aspects:

1. Having correct simulation outputs (frequency, total power output, voltage to the load)
2. Showing frequency stability in the simulation
3. Demonstrating the control ability of output power and voltage
4. Building a different droop controller integrated with virtual inertia

Chapter Two: Design of Microgrid

2.1 General Structure of Microgrid

This islanded microgrid is composed of the DG, the distribution network, the control system and the load. More specifically, the distributed generators are composed of the Photovoltaic (PV) system and the wind turbine system so this microgrid uses renewable energy as the resource. Both the PV system and the wind power system have their own control system. The general structure of the microgrid is shown in the Figure 2.1 below:

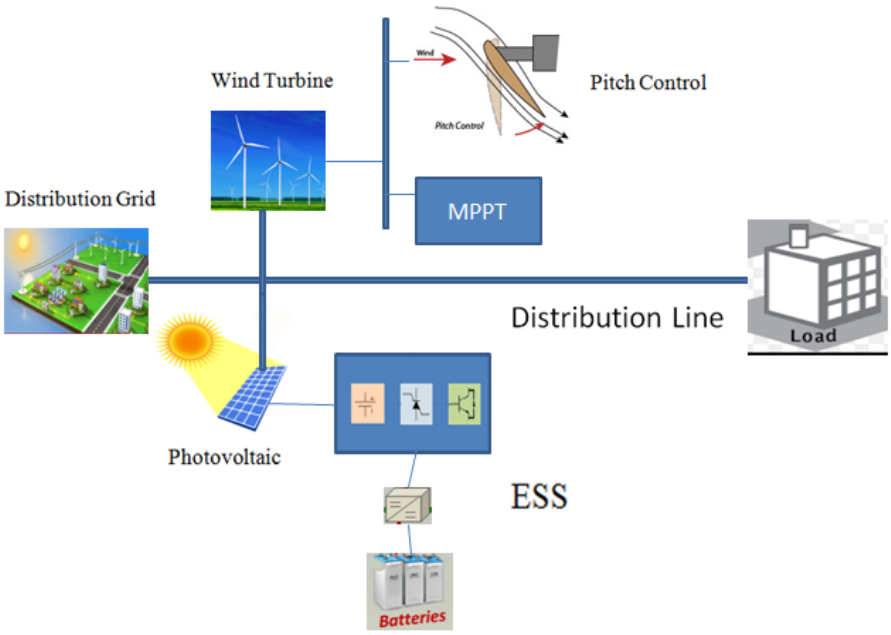

Figure 2.1 Structure of the Microgrid

Figure 2.1 shows the basic structure of the microgrid, which includes the distribution grid, the wind turbine equipped with the pitch controller and the MPPT controller, the photovoltaic, the energy storage system, the battery, the distribution lines and the load. The distributed generators use wind and solar as resources. The ESS which includes the converter and the battery is used to supply or assimilate power. In terms of the control of the wind power system, the pitch controller and the MPPT control are included. Finally, the distribution lines and the load are also added as the indispensable components of the microgrid.

In terms of the PV system, each solar panel is comprised of a number of solar cells that generate electric power [28]. PV panel converses light into electricity and it produces no pollution; this technology has been used since half a century ago and is getting cheaper and more efficient nowadays. The PV system also includes the converter that connects the panels and the inverter. Furthermore, an energy storage system is also built to provide power to the load when there is no sunlight and the irradiance becomes 0.

Wind turbine converts kinetic energy of the wind into electric power and it can be manufactured in both vertical and horizontal axis types [28]. The small and medium sized wind turbines are used for applications such as battery charging for auxiliary power for boats or supplying domestic power while selling unused power back to the utility supplier via the electrical grid [29]. Arrays of large turbines, known as wind farms, are used as the main source of renewable energy and are used by many countries as the replacement of fossil fuels and oil [30].

Since most of the wind plants in the microgrid are composed of variable-speed and horizontal axis wind turbines, this thesis also chooses the same type (variable-speed and horizontal axis) as the wind turbine.

The block diagram of microgrid in details is shown in figure 2.2 as below:

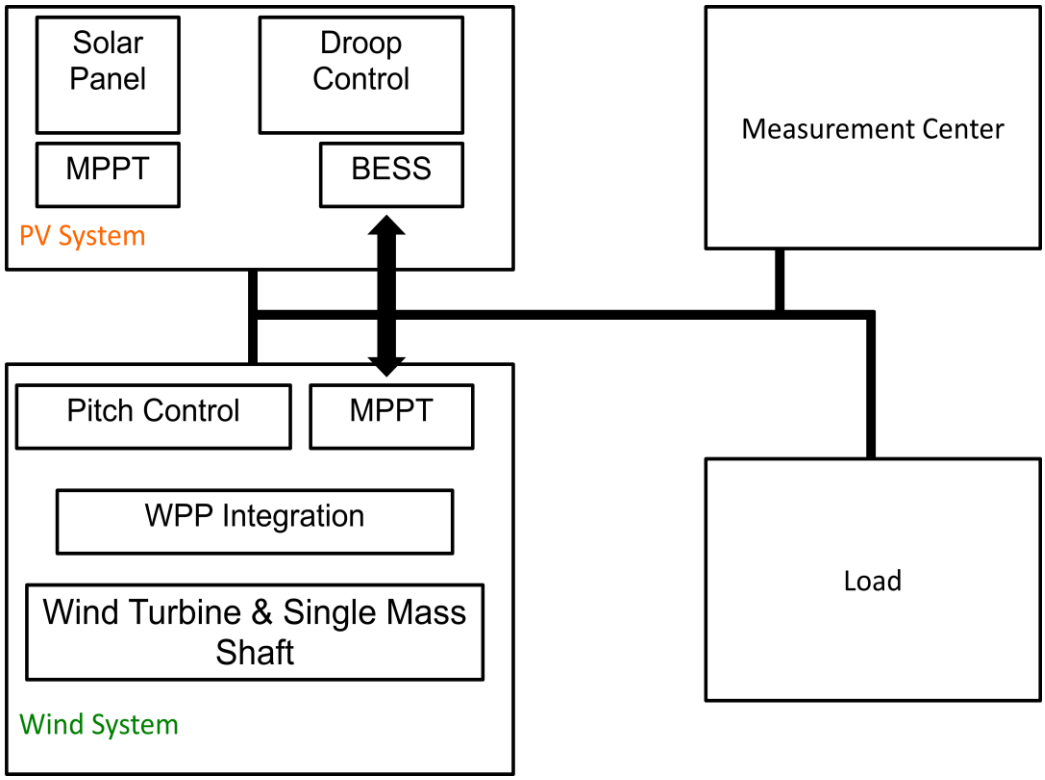

Figure 2.2 Block Diagram of the Microgrid in Details

This is the architecture of the microgrid system and it includes two distributed generators (PV and wind turbine). The battery energy storage system (BESS) of PV system and the MPPT of wind power system can communicate with each other so the microgrid can be controlled coordinately. This microgrid system can be connected or disconnected to the distribution grid. When the distribution grid has been disconnected, the microgrid can provide power to the local load.

2.2 Specific Design of the PV System

The first step is to design the PV system. The block diagram structure of the PV system is shown in Figure 2.3 as below:

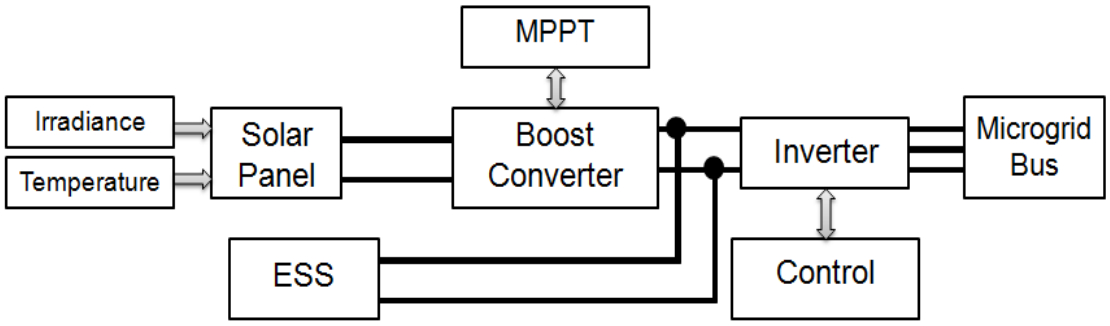

Figure 2.3 Structure of the PV System

The output of the solar panel is dictated by the solar irradiance and the environmental temperature. In this case, we assume the temperature is 15 degrees Celsius. The output solar panel the dc power into the boost converter so boost converter can regulate output solar panel based on the MPPT controller. Then the DC power is sent to the inverter system, which is controlled by the droop control system so the AC power is delivered to the microgrid bus. The battery energy system can be charged or discharged according to the solar panel output.

From Figure 2.3, it is clearly seen that the PV system is composed of the PV panel, the control system, the MPPT and the Energy Storage System (ESS). In MPPT, it tracks the maximum power output of the solar panel; droop controller decides the output power of overall PV system, and BESS can be charged/discharged based on the output

power of the solar panel. When the PV panel cannot output enough power, the BESS discharges itself to meet the demand for the power output.

The equivalent circuit of the PV cell is based on the model as shown in Figure 2.4 as below:

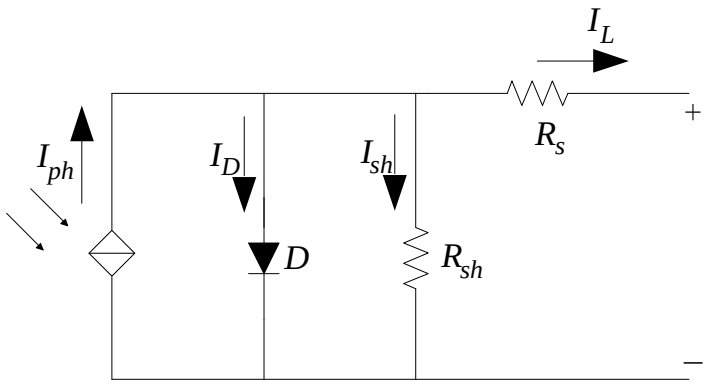

Figure 2.4 Equivalent Circuit of the PV Array

As the figure shows above, I_{ph} is the photocurrent, I_D is the current of the diode, R_{sh} is the shunt resistance and R_s is the series resistance, and I_{sh} represents the shunt current. Based on the photoelectric effect, the equation of I_{ph} can be represented as below [31]:

$$I_{ph} = \frac{[I_{sc}+K_t(T-T_{ref})]S}{\lambda} \tag{2.1}$$

where S represents the solar radiation, I_{sc} is the short-circuit current at the standard temperature. K_t represents the short-circuit current temperature coefficient of the cell. T_{ref} is the reference temperature and λ has the value of 1000 W/m^2. Based on the characteristics of diode, the equation of the I_D can be represented as (2.2) and the relation of the voltage and current of p-n junction can be represented as equation 2.3:

$$I_D = I_0(e^{\frac{qV}{AKT}} - 1) \tag{2.2}$$

$$V = I_{sh}R_{sh} + I_L R_s \tag{2.3}$$

where q has the value of 1.6e-19 C and K = 1.38e-23. I_0 is the reverse saturation current. Based on equations 2.1, 2.2 and 2.3, the characteristic equation for the voltage-current of a solar cell is given as [31]:

$$I_L = I_{ph} - I_0\left(e^{\frac{q(V_{DC}+I_L R_L)}{AKT}} - 1\right) - \frac{V_{DC}+I_L R_L}{R_{sh}} \tag{2.4}$$

In order increase the capacity of the output power of the PV array, multiple photovoltaic cells are interconnected in parallel and series to have desired volt-ampere characteristics of the entire photovoltaic cell array. The revised equation is given as [31]:

$$I_L = N_p I_{ph} - N_s\left(e^{\frac{q(V_{DC}+I_L R_L)}{AKT}} - 1\right) - \frac{V_{DC}+I_L R_L}{R_{sh}} \tag{2.5}$$

where N_p is the number of PV cells that are connected in parallel; N_s is the number of PV cells in series. Also, the cell's saturation current varies with the temperature of the cell as described in the equation shown below [31]:

$$I_S = I_{RS}(T_C - T_{ref})^3 * e^{qE_G(\frac{1}{T_{ref}} - \frac{1}{T_C})/AK} \tag{2.6}$$

Where E_G is the band-gap energy of the semiconductor in the PV cell [31].

The boost converter is designed as a step-up converter that aims to increase the voltage to a higher output value. In this case, the output solar panel the DC power into the boost converter, so the boost converter can regulate output solar panel based on MPPT controller.

The algorithm of the MPPT is illustrated in the figure as shown below:

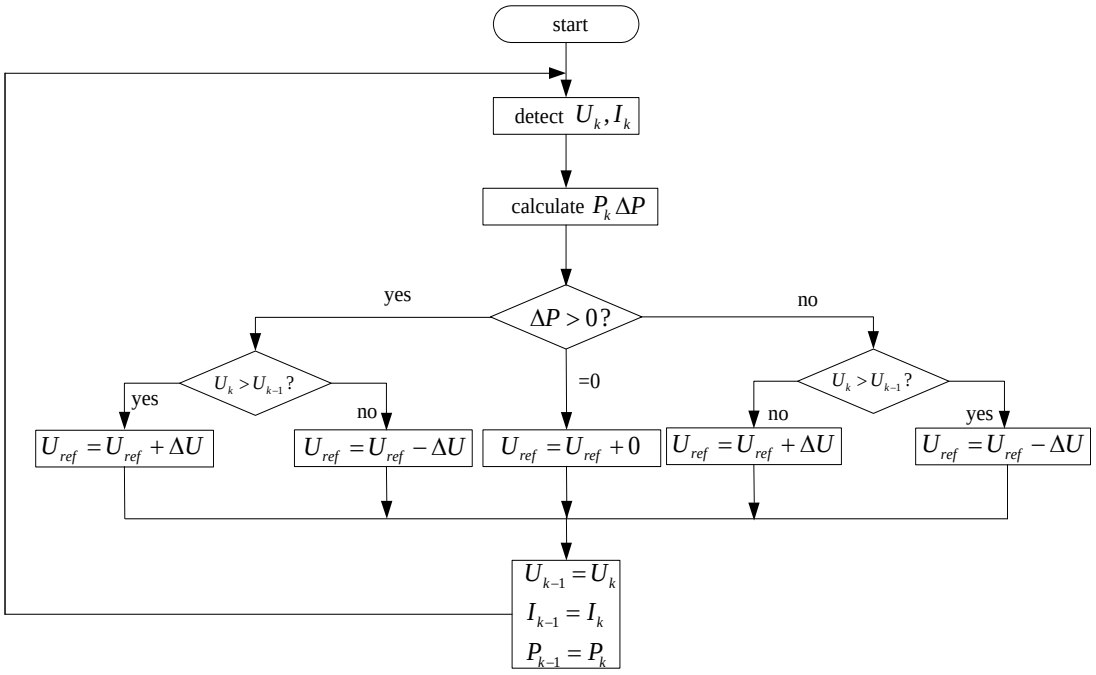

Figure 2.5 Algorithm of the Perturb & Observe Method

It is explained in Figure 2.5 that the MPPT controller uses the Perturb & Observe method in PV system. Basically, the output power is changed due to the perturbation of the array voltage and it is compared with that of the previous cycle. The perturbation continues in the same direction if the power increases due to the perturbation and the perturbation reverses the direction if the peak power reaches the power at the maximum power point [32]; therefore, the output power keeps oscillating around the maximum power point.

2.3 Battery Energy Storage System

It is very challenging to control and operate the renewable microgrid due to the variability and intermittency of distributed generators that use renewable energy. Therefore, an energy storage system (ESS) is necessary in the PV system. The ESS can provide the specific voltage and frequency support for the islanded microgrid and it changes the power output to regulate the frequency and voltage to the scheduled values [32]. Therefore, the Energy Storage System plays a vital rule in stabilizing the microgrid.

There are various types of converters in the Energy Storage System, such as DC-DC and DC-AC converters. Since solar panel outputs DC power, a DC-DC converter is used in this case in order to change the voltage level. The buck-boost converter is indispensable because it is able to both charge and discharge the Battery Energy Storage System (BESS), therefore changing the direction of the power flow according to different situations. For instance, the voltage of the energy storage system will be stepped up when its voltage is lower than that of the microgrid side so that the battery energy storage system can discharge to supply power to the microgrid and vice versa [33].

In this thesis, the battery energy storage system consists of one buck-boost bidirectional converter and one battery; the structure of the converter is shown in Figure 2.6 as below:

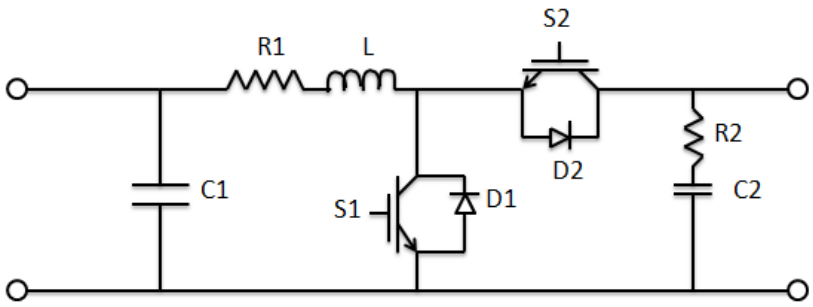

Figure 2.6 Structure of the Buck-Boost Bidirectional Converter

Power allocation is achieved by controlling the direction and value of the electrical power flowing through the bi-directional dc/dc converter. *C1* is the low-voltage side and *C2* is the high-voltage side.

As it is shown above, the inductance is 2.332 mH and the diode has the resistance of 0.001 ohm, forward voltage of 0.3 V. Both the MOSFET and internal diode have the resistance of 1 ohm. Basically, when MOSFET1 (*S1*) is switching, and MOSFET2 (*S2*) is kept on and it is the boost converter; the battery discharges the energy to the microgrid. When *S1* is OFF, *S2* is switching, it is the buck converter and the battery is getting charged [34].

The other component of the battery energy storage system is the battery. The battery type is the Lithium-ion in this case. One of the reasons to choose this type of battery is that Lithium-ion battery is a very popular type of rechargeable battery with a high energy density, tiny memory effect and low self-discharge [35]. The nominal voltage is set to be 311 volts and the rated capacity is set to be 1000 Ah with the maximum capacity of 1077 Ah. Therefore, the battery has an appropriate capacity that is neither too large nor too small based on these values.

The output of the boost converter goes to the VSC, voltage source converter and the circuit is shown in Figure 2.7 as below:

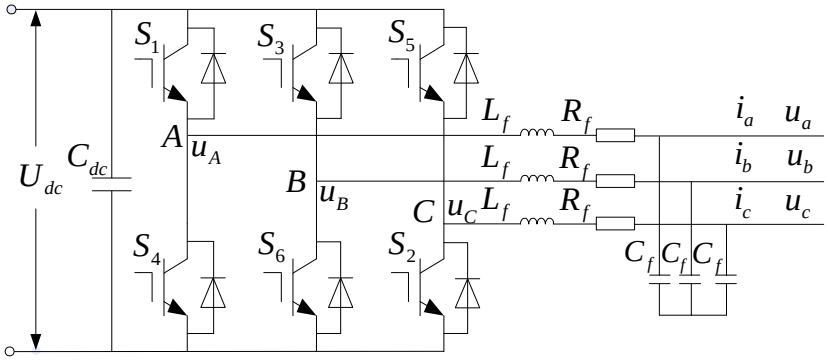

Figure 2.7 Circuit of the Voltage Source Converter

As the figure shows, there are six switches (S1 to S6) paired with six diodes in the three-phase voltage inverter. U_{dc} is the direct output voltage from the solar panel, C_{dc} is the filter capacitor, L_f is the filter inductor and R_f is the filter resistance. u_a, u_b, u_c represent the output voltages of the inverter and i_a, i_b, i_c represent the output currents of the inverter.

2.4 Control System of PV

The control system of PV is also significant. The control system is expected to control the frequency, the output power and the voltage in the PV system. The structures of the PV control system are shown in Figure 2.8:

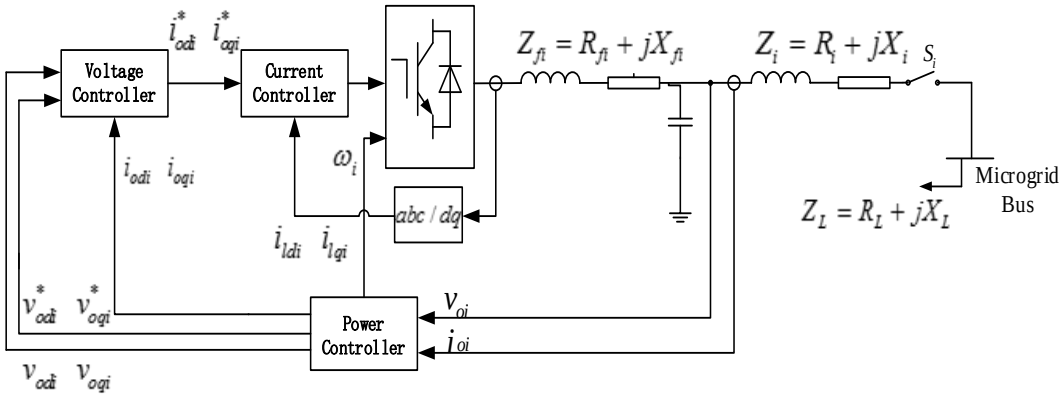

Figure 2.8 Structure of the PV Control System

As it is shown above, the PV control system calculates the power output of the VSC using feedback signals V_{abc} and I_{abc}, then droop controller can generate reference signal so the voltage and frequency of microgrid can be regulated. Then the reference signals are sent to the dual-loop PI controller in which the outer loop is voltage PI controller and the inner loop is the current PI controller. The dual-loop PI controller has the structures as shown below:

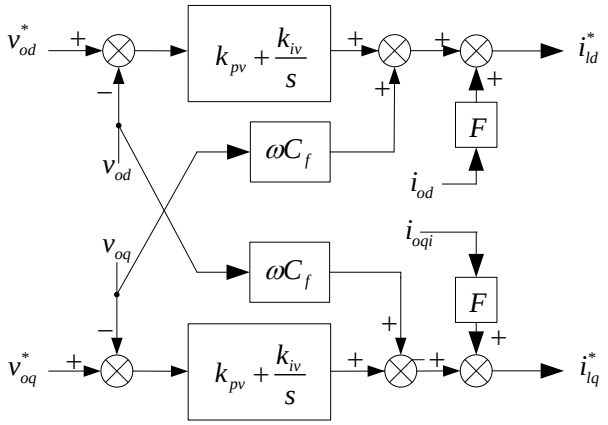

Figure 2.9 Structure of the Voltage Controller

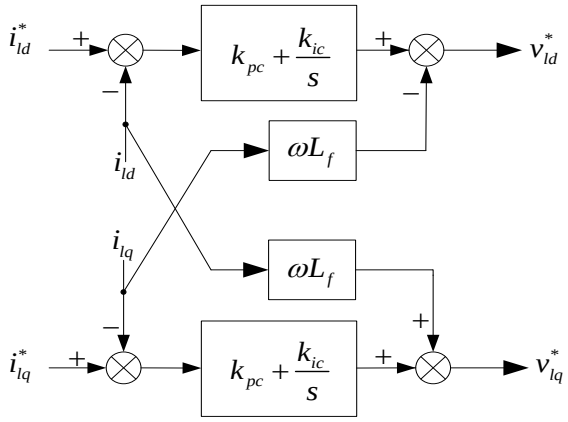

Figure 2.10 Structure of the Current Controller

There is coupling effect when converting the three-phase voltage and current of the VSC into the voltage and current of d-axis and q-axis, so the decoupling terms ($\omega C_f v_{oq}, \omega C_f v_{od}, \omega L_f i_{iq}, \omega L_f i_{id}$) are added in the voltage and current controller [36]. In Figure 2.9, the structure of the voltage controller is based on the equations as shown below:

$$\varphi_{vd} = v_{od}^* - v_{od} \tag{2.7}$$

$$\varphi_{vq} = v_{oq}^* - v_{oq} \tag{2.8}$$

$$i_{id}^* = i_{od}F - \omega C_f v_{oq} + k_{pv}(v_{od}^* - v_{od}) + k_{iv}\varphi_{vd} \tag{2.9}$$

$$i_{iq}^* = i_{oq}F - \omega C_f v_{od} + k_{pv}\left(v_{oq}^* - v_{oq}\right) + k_{iv}\varphi_{vq} \tag{2.10}$$

Where φ_{vd} and φ_{vq} represent auxiliary variables and k_{pv} and k_{iv} are the regulating parameters of voltage controller. Similarly, the equations of the current controller in the PI controller are shown below:

$$\varphi_{id} = i_{id}^* - i_{id} \tag{2.11}$$

$$\varphi_{iq} = i_{iq}^* - i_{iq} \tag{2.12}$$

$$i_{id}^{*} = k_{pc}(i_{id}^{*} - i_{id}) + k_{ic}\varphi_{id} - \omega L_f i_{iq} \tag{2.13}$$

$$i_{iq}^{*} = k_{pc}\left(i_{iq}^{*} - i_{iq}\right) + k_{ic}\varphi_{iq} - \omega L_f i_{id} \tag{2.14}$$

where φ_{id} and φ_{iq} represent auxiliary variables and k_{pc} and k_{ic} are the regulating parameters of current controller.

2.5 Droop controller integrated with virtual inertia

In this case, a droop controller integrated with virtual inertia is designed. The inspiration of this droop controller comes from the technique of virtual synchronous machine (VSM), which controls the grid-interface converter of the distributed generator to imitate the characteristics of the synchronous generator [37]-[45]. The droop controller supervises the frequency and power by controlling the frequency and voltage based on the two equations as below:

$$f = f_0 - m(P - P_0) \tag{2.15}$$

$$V = V_0 - n(Q - Q_0) \tag{2.16}$$

Where f_0 and V_0 represent the base frequency and the base reference voltage; Q_0 and P_0 are the base reactive and active power of the unit, m is the frequency droop coefficient and n is the voltage droop control coefficient[46].

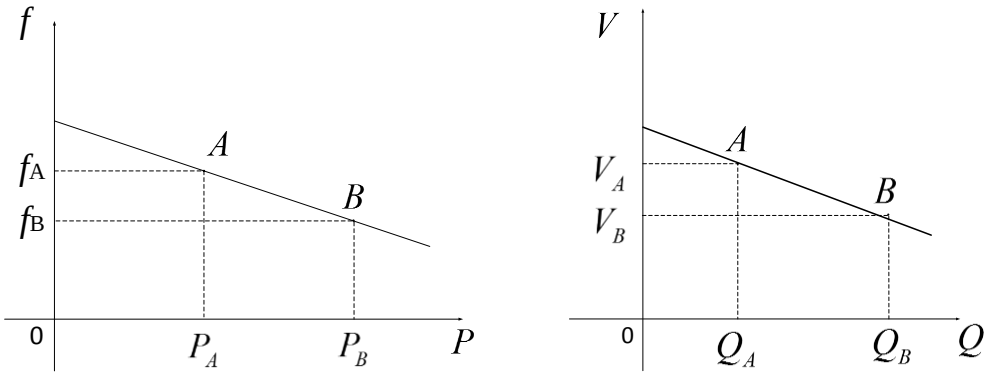

(a) Frequency Droop Characteristic **(b) Voltage Droop Characteristic**

Figure 2.11 Droop Characteristic of Distributed Generators

Figure 2.11 (a) and (b) explain the *P-f* droop characteristic and *Q-V* droop characteristic respectively. In figure (a), when frequency falls from f_A to f_B, the power reference of the distributed generator increases from P_A to P_B. The decrease of frequency indicates the increase in the load. The active power is increased to counteract the reduction in frequency so the units will settle at active power outputs and frequency at a steady-state point on the frequency droop characteristic. This logic can be applied to the voltage droop characteristic as well. However, this kind of frequency droop controller cannot perfectly handle a situation when there is a significant emergency such as the loss of a large generating unit. This is because when the large generating unit is lost suddenly, the droop characteristic allows the frequency to settle below its nominal value when all the units pick up the slack [46].

By contrast, this modified controller uses the characteristics of virtual inertia to control the frequency and power based on this equation:

$$T_e - T_m = J\frac{d\omega}{dt}D_p(\omega - \omega_n) \tag{2.17}$$

The purpose of integrating virtual inertia into droop controller is to let the PV system imitate the behavior of the traditional synchronous generator. Therefore the droop controller integrated with the virtual inertia can provide inertia response when the load of the microgrid system suddenly changed. The structure of the droop controller integrated with virtual inertia is shown as below:

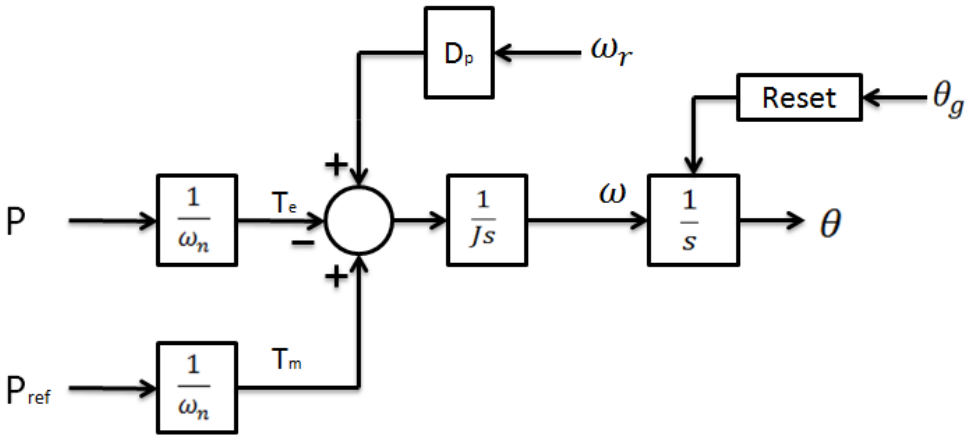

Figure 2.12 Structure of the Droop controller Integrated with Virtual Inertia

This controller is able to control the frequency deviation in a smaller range compared to that of the droop controller without virtual inertia; this is because the virtual inertia based droop controller can boost a larger reference power in a short time when the frequency drops suddenly, thus curtailing the droop speed of frequency . Therefore, the droop controller integrated with virtual inertia avoids the drawback of the common droop controller and has better control of frequency stability.

The input values of *P* and *Q* are compared with the reference values (3000 Watts for *P* and 500 Var for *Q*) of *P* and *Q* respectively; Using the equation $P = T\omega$, the active power and the reference power are divided by $2\pi f$ respectively (frequency is 60 Hz by

American Standard) to get the electrical torque and mechanical torque. Then the values of T_e and T_m are sent to the synchronous generator swing equation to get the value of ω and Θ. D_p represent the sum of the frequency-droop coefficient and the imaginary mechanical-friction coefficient [47]. After that the frequency is calculated by the equation $f = 2\pi\omega t$. The output values ω and Θ of the droop control system are sent to the dual-loop PI controller which is explained in section 2.4.

The following is the test case comparing the frequency control using regular droop controller to that using the new droop control. The power of the load is changed from 2 kW to 3 kW at 2s and the frequency data are simulated as shown in Figure 2.13 below:

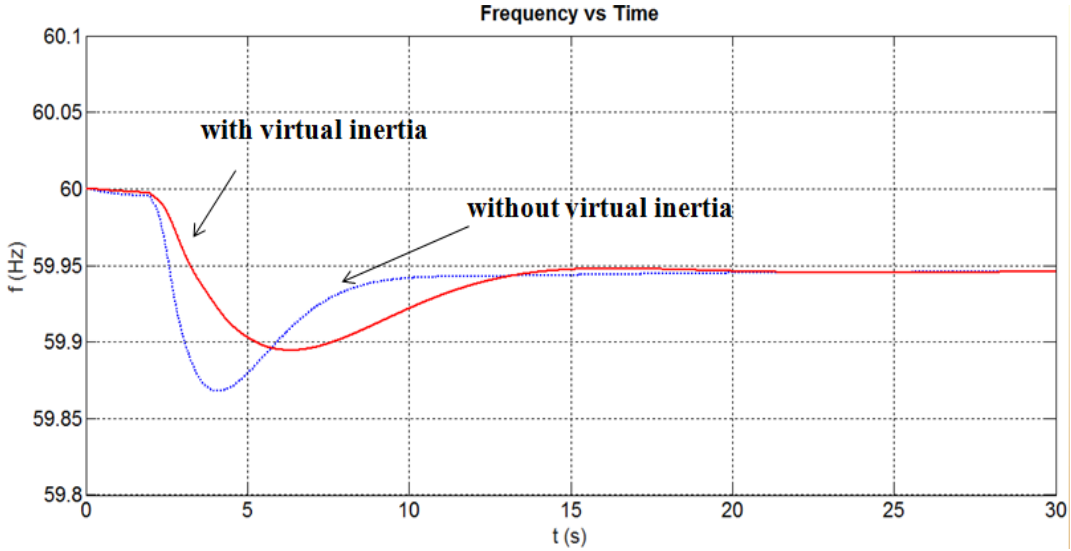

Figure 2.13 Frequency Control under Two Droop Controllers

In Figure 2.13, the red line is the frequency controlled by the droop controller integrated with virtual inertia and the blue line is the frequency controlled by the droop controller without virtual inertia. As it is shown, the frequency deviates 0.135 Hz under the control of the droop controller and 0.107 Hz under the droop controller integrated

with virtual inertia, which means that the frequency deviation is 21% less using the droop controller integrated with virtual inertia than using the droop controller without virtual inertia. Therefore, the virtual inertia based droop controller has better frequency stability control than that of the droop controller without virtual inertia.

Chapter 3 Wind Power System

3.1 Introduction to Wind Power System

The second distributed renewable source is the wind energy conversion system (WECS). Variable-speed Wind Turbine Generator (WTG) is controlled by the power converter that is interfaced between the WTG and grid. There are two types of variable-speed WTGs, doubly fed induction generator (DFIG) and permanent magnetic synchronous generator (PMSG). In comparison with a doubly fed induction generator, a PMSG-WTG has higher efficiency and reliability because it can be driven directly by a wind turbine since the rotating speed of the generator is slowed down with the multi-pole structure. On the other hand, the PMSG is also expensive for its high cost of converter [49]. Since this thesis focuses on the small-sized grid, the PMSG is used here as the type of wind turbine generator. The typical structure of the PMSG is shown in figure 3.1as below:

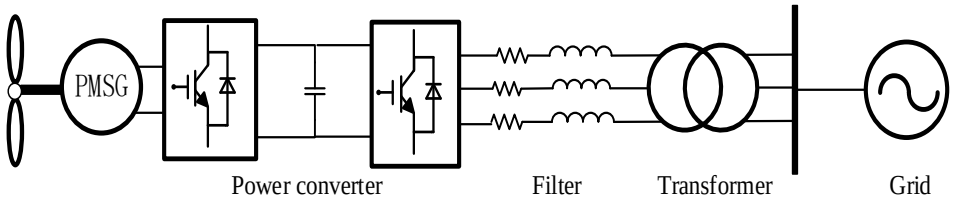

Figure 3.1 Structure of PMSG

In PMSG, the air gap flux is maintained by the permanent magnet and only the q-axis current decides the electrical torque because there is the d-axis current controlled to

be 0 by the generator-side converter (GSC) [49]. In this thesis, the wind power system is composed of the wind turbine and single mass shaft, the Wind Power Plant (WPP) Integration, the MPPT controller and the pitch controller.

3.2 Wind Aerodynamic and Single Mass Shaft

The wind aerodynamic and single mass shaft have the structure as shown below:

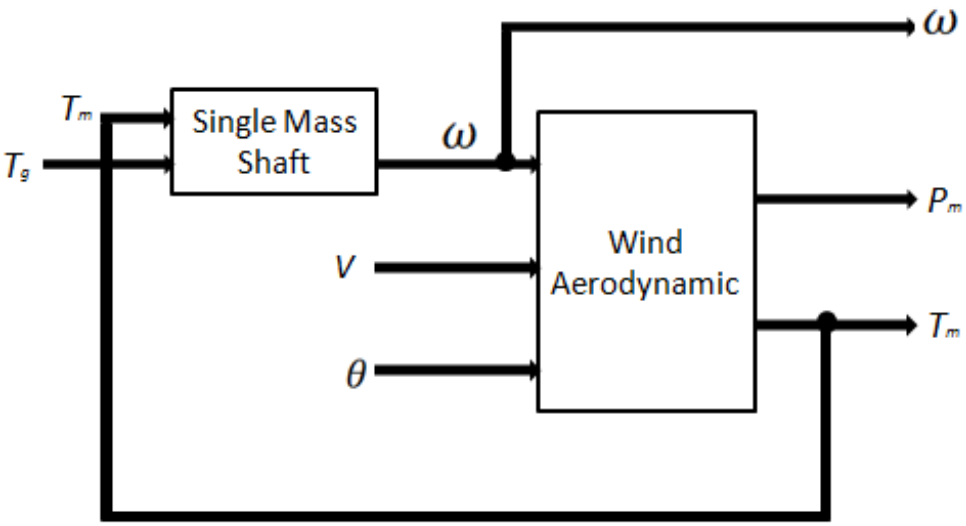

Figure 3.2 Structure of the Wind Aerodynamic and Single Mass Shaft

As it is shown in Figure 3.2, there are two conversion processes in the wind turbine generator. The wind turbine gets the torque from the pressure of the wind and the mechanical torque is converted into electric power through the generator [49].

The single mass shaft is based on the equation below:

$$T_\tau - T_g = 2H\frac{dw}{dt} \tag{3.1}$$

The difference between the wind turbine torque and the generator torque is in proportional to $\Delta\omega$. H has the value of 3 and then using the equation of rotor speed $\Delta\omega +$

$\omega_0 = \omega$, where $\omega_0 = 0.5$ and is added to the speed to calculate the rotor speed, which is sent to the wind turbine.

The wind aerodynamic function is based on equation 3.2 as shown below:

$$P_m = \frac{1}{2}\rho\pi R^2 v^3 C_p(\boldsymbol{\lambda}, \theta) \tag{3.2}$$

The power of the wind turbine is in proportional to the air density (ρ), the area of the turbine blade (πR^2), the wind speed (v) and the power coefficient of the blade ($C_p(\boldsymbol{\lambda}, \theta)$). The air density is 1.225 kg/m^3 and radius of the blade is 39.26 m. The power coefficient is also related to the tip speed ratio (TSR) $\boldsymbol{\lambda}$ and the pitch angle θ; where $\boldsymbol{\lambda} = \frac{\omega R}{v}$. Therefore, it is necessary to adjust the turbine speed according to the wind speed in order to get the maximum power and conversion efficiency.

According to the Betz limit, the power coefficient of the blade has a theoretical maximum value of 0.59. Then the value of the power coefficient of the blade ($C_p(\boldsymbol{\lambda}, \theta)$) is figured out by the value of $\boldsymbol{\lambda}$ and the value of the pitch angle θ.

3.3 MPPT Controller and Pitch Angle Controller

In the control system of the WTG, the MPPT controller and the pitch controller work coordinately. The control of a variable-speed wind turbine below the rated wind speed is achieved by controlling the generator [50]. The maximum power coefficient, $C_{p,max,}$, is related to the optimal value of $\boldsymbol{\lambda}$ and pitch angle θ. Thus, the rotor speed is controlled to maximize the power extraction from the wind and the MPPT controller is needed. The MPPT controller is based on the equations 3.3 and 3.4:

$$P_l = K\omega^3 \tag{3.3}$$

$$K = \frac{1}{2}\rho\pi R^5 \frac{C_{p,max}}{\lambda_{opt}{}^3} \quad (3.4)$$

From equation 3.3 and 3.4, the power extraction is in proportional to the cube of the rotor speed. A pitch controller is also designed to maintain the optimal rotor speed $\boldsymbol{\lambda}_{opt}$ according to the wind speed measurement by controlling the pitch angle. Basically, the pitch controller restricts the mechanical power output by changing the pitch angle of the blades so the rotor speed is controlled within the limit when the wind speed exceeds the rated value.

The basic structure of the pitch controller is shown as below:

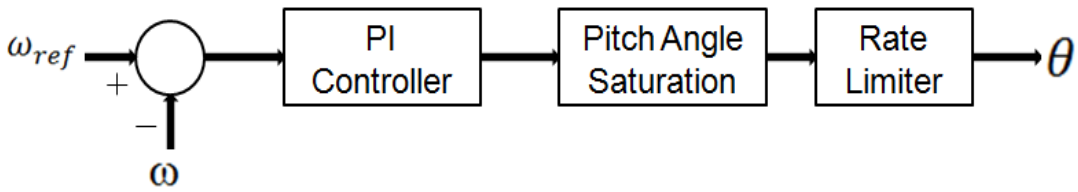

Figure 3.3 Structure of Pitch Controller

As it is shown from the Figure 3.3, the pitch controller is capable of restricting the rotor speed under high wind speed by turning the blade angle of attack and it is clamped to the optimal value, which is set to be 0 degrees when the wind speed is below the rated value [51]. When the wind speed exceeds the speed of the rated value, the pitch controller increases the angle of the attack of the blade, therefore making the reduction in the lift force; when the blade is fully pitched, the pitch controller makes the blade angle of attack aligned with the wind so that the lift force is zero in this occasion, thus reducing the loads on the turbine mechanical components and avoiding a run-away condition [51]. The pitch angle saturation and the rate limiter are also added into the pitch controller, in which the

pitch angle ranges from 0 to 30 degrees and the pitch rate limit is set to be 10 degree/second. Therefore it prevents the blades from damaging due to frequently operating the blades.

3.4 WPP Integration

A complete WECS integration model is composed of the PMSG and back-to-back full power converter [52]. In [52], the simplified generator in the wind turbine model and back-to-back average power converter constitute a complete PMSG integrated model. The PMSG and power converters can be either mathematical model or built-in blocks of SimPowerSystems in Simulink. In this thesis, a simplified mathematic model is designed to integrate into the wind turbine using the controlled current source. The inner structure of wind power plant (WPP) Integration is shown in Figure 3.4 [52]:

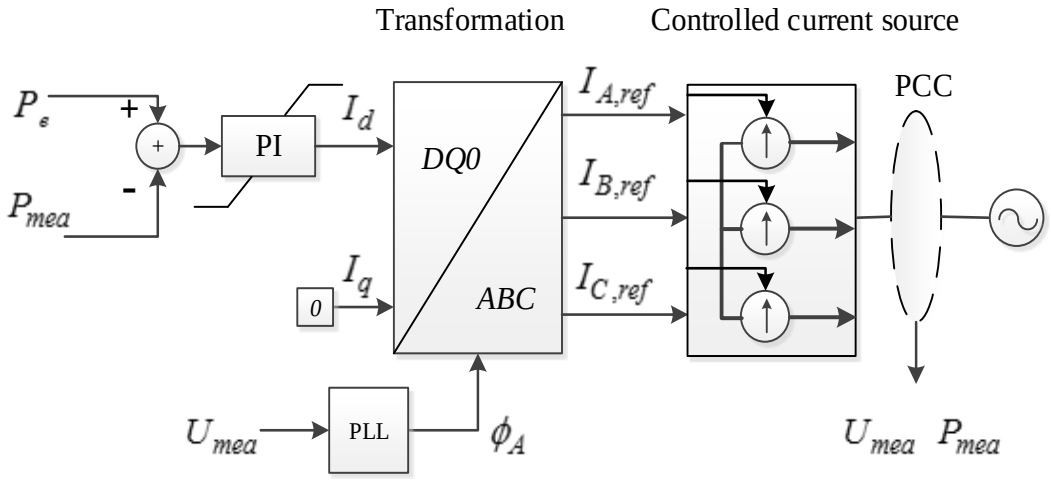

Figure 3.4 WPP Integration

From Figure 3.4, it is shown that the WPP integration gets the input from the MPPT controller and outputs the three phase current I_A, I_B and I_C through the controlled current source. The d-axis current is controlled by the PI controller according to the difference between the measured power and the power reference [52]. A power measurement block is used in the WPP integration to transform voltage and current to the active power and reactive power using the equations shown below:

$$U(t) = \sqrt{2}U_{rms}\sin(wt + \varphi) \tag{3.5}$$

$$I(t) = \sqrt{2}I_{rms}\sin(wt + \theta) \tag{3.6}$$

$$P = 3U_{rms}I_{rms}\sin\theta \tag{3.7}$$

The phases of three phase voltage and current are 120 degrees apart; since U_{rms} is constant, we can calculate the rms value of the current using the equation:

$$I_{rms} = \frac{P}{3U_{rms}\sin\theta} \tag{3.8}$$

The value of I_{rms} is calculated using the value of the power, the voltage and the phase angle.

Chapter Four: Testing Results

4.1 System Description

In order to test the control system under different conditions, the thesis provides five different test cases. Case 1 to case 3 are based on 2kW load, case 4 and 5 are based on 3 kW load. The details of the five cases are shown in Table 1:

Table 4.1 Simulation Cases

	Irradiance	Wind Speed	Load
Case 1	High	High	Load 1
Case 2	Moderate	Moderate	
Case 3	Very Low	Low	
Case 4	Fluctuate	Very High	Load 2
Case 5	Very Low	Low	

As the table shows, case 1 to 5 have different intensities of irradiance and wind speed, therefore showing the tests of control system under different conditions of the environment. The two different loads also test the control system under different loads. The reason to choose the small-sized load is that this thesis focuses on the power supply for the household. In terms of the load, the phase-to-phase voltage V_{rms} is set to be 380 volts and the frequency is 60 Hz. The simulation time step is 5 us and the total simulation

time is set to be 30s. In each of the cases, the frequency of the microgrid, the total power output and the voltage to the load are tested and compared.

4.2 Load 1

4.2.1 Case 1

In case 1, the solar radiation is high at daylight (800 W/m^2) and the wind speed is high as well (11m/s). The frequency and total output power of the islanded microgrid system are shown as below:

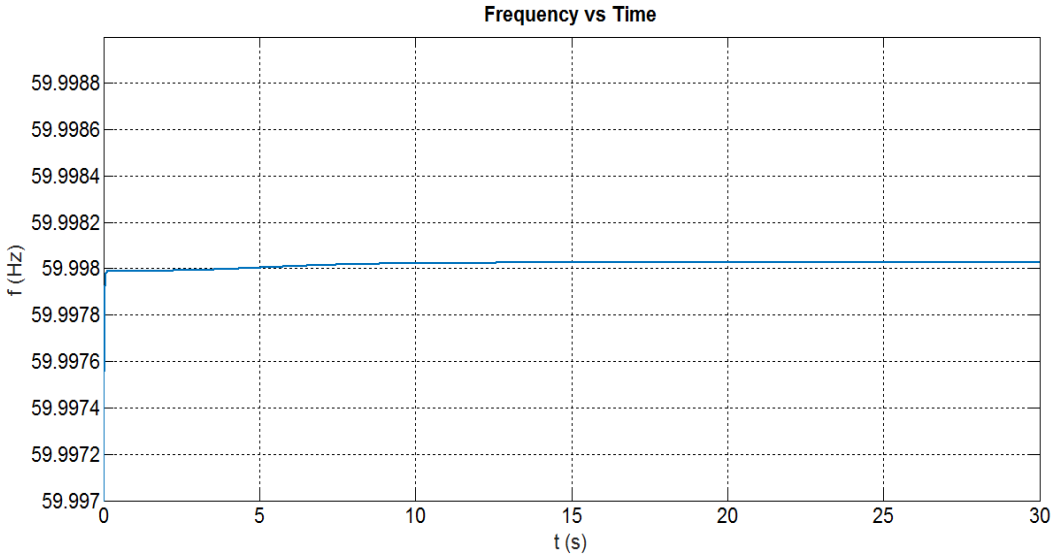

Figure 4.1 Frequency of the Microgrid

As shown in the Figure 4.1, the frequency of the microgrid is kept at around 59.998 Hz steadily after 10s, which is very close to the ideal value 60 Hz. This proves the precise control of the frequency. Next test aspect is the total power output from the wind power system and the PV system, which has the result as shown in the figure below:

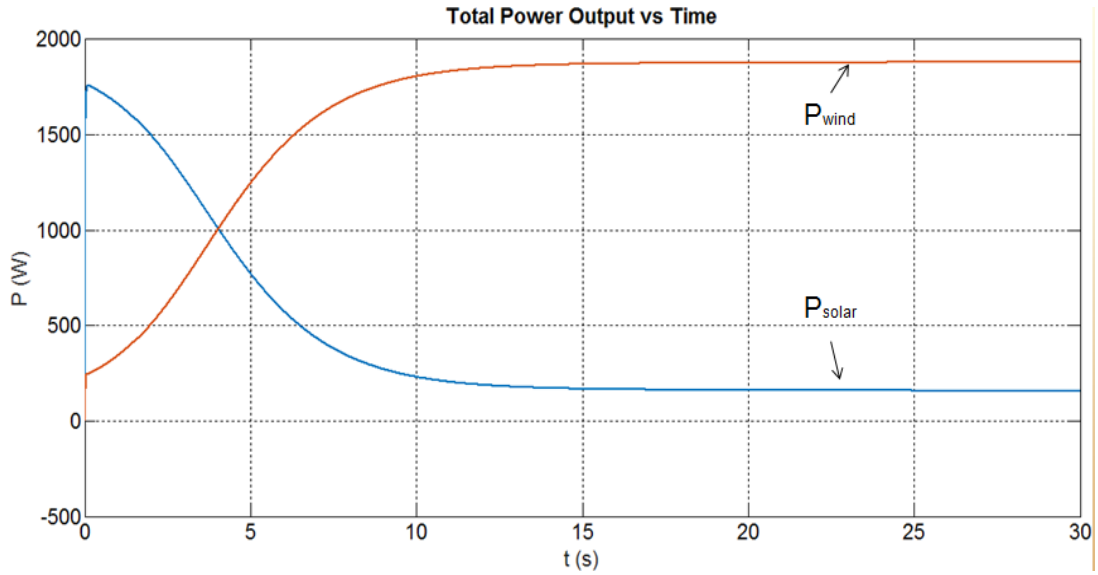

Figure 4.2 Total Power Output of the Microgrid

In Figure 4.2, the x-axis indicates the time and the y-axis represents the power. Clearly, the PV system output starts at around 1750 W first and then decreases steadily while the wind power plant starts with 200 W and increases with time; both PV system and the wind power plant output steadily after 12s, where WPP provides 1880 W and the PV system provides around 170 W, giving the total of around 2050 W to the load. The constant value of the grid frequency indicates the balance between the active power output of distributed generators and that of the loads. Since the PV and wind power system are operated to track the maximum power points, the droop control implemented in the ESS is important to maintain the power balance. As shown in Fig. 4.2, the power output of PV system is reduced by charging the battery to meet the consumption of loads due to the high wind power generation. Therefore, the control of the output power is proved to be successful.

Next is the test of the voltage to the load, the test result is shown in the figure below:

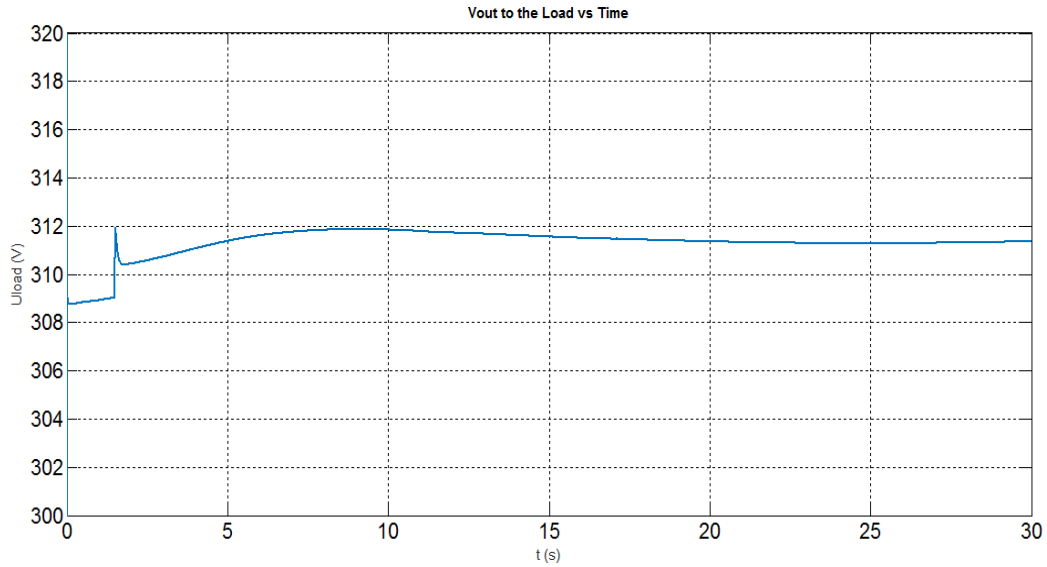

Figure 4.3 Output Voltage to the load

In Figure 4.3, the output voltage sent to the load fluctuates at first and then keeps at around 311 Volts. Using the equation $380\frac{\sqrt{2}}{\sqrt{3}} = 311\ V$, it is proved that the voltage output is the nominal value.

4.2.2 Testing Case 2

In case 2, both the wind speed and the irradiance of the solar are moderate. The wind speed is 7m/s and the solar radiation is between 400 W/m^2 and 600 W/m^2 in this case. The test results of the frequency, the total output power and the voltage to the load are shown as below:

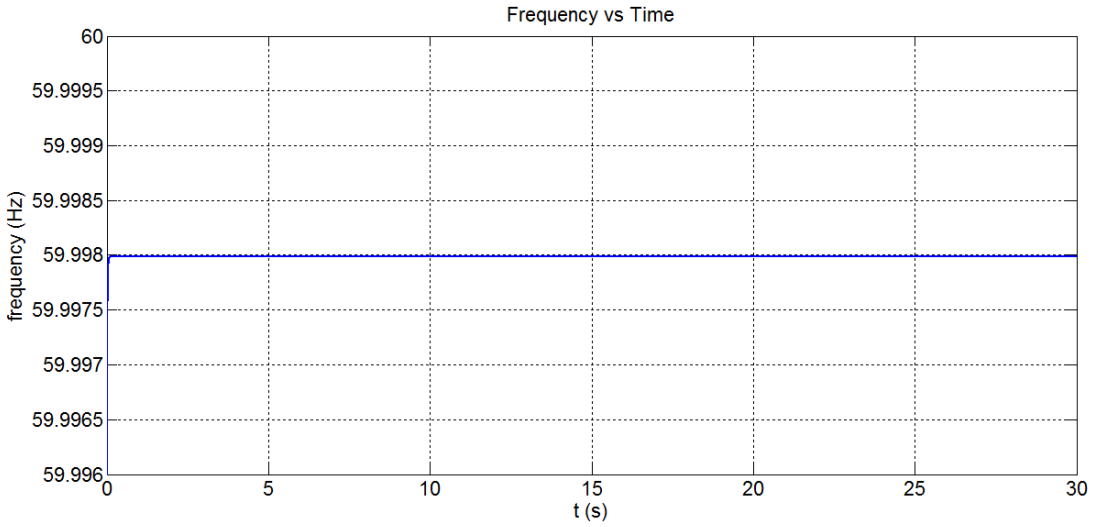

Figure 4.4 Frequency of the Microgrid

As shown in the Figure 4.4, the frequency of the microgrid is kept at around 59.998 Hz steadily from the start to the end, which proves the precise control of the frequency as well. Next are the total power output and the RMS voltage to the load:

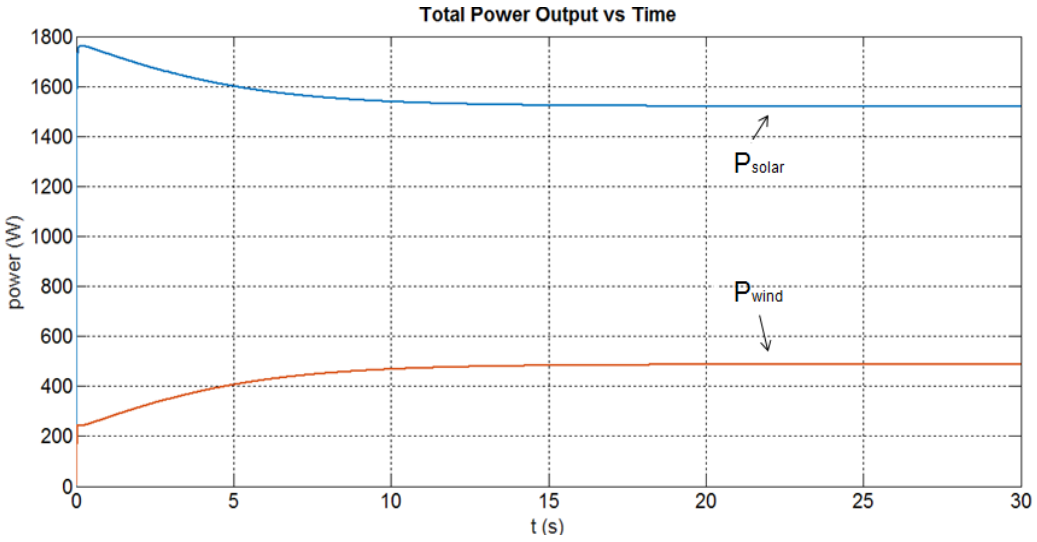

Figure 4.5 Total Power Output

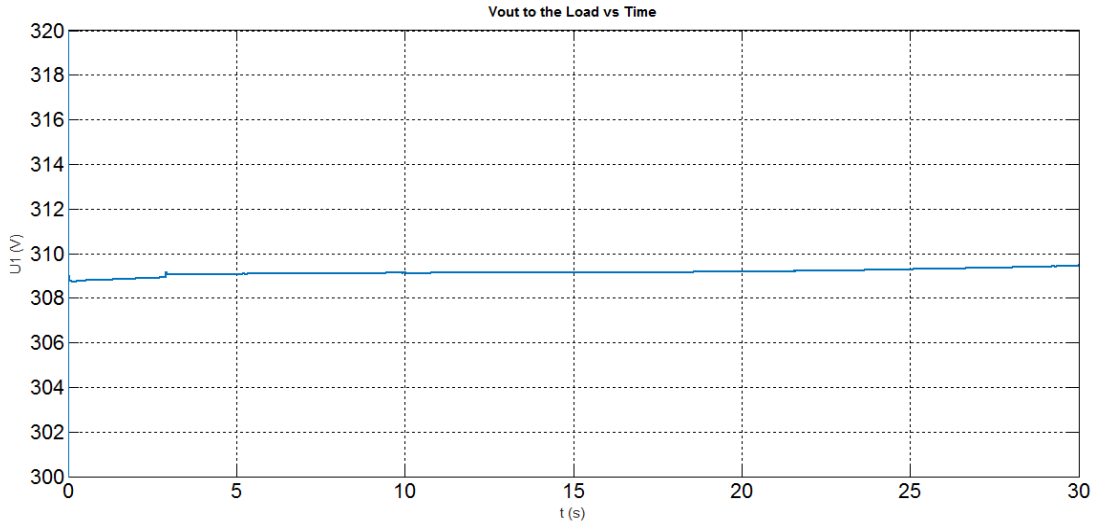

Figure 4.6 RMS Voltage to the load

From Figure 4.5 and 4.6, it is shown that the output of the power system starts at around 1750 W first and then decreases steadily while the wind power system starts with 0 and increases with time slowly; both PV system and the wind power plant output steadily after 12s; where WPP provides about 487.8 W and the PV system provides around 1550 W; giving the total of 2037.8 W to the load. From Figure 4.6, the RMS voltage to the load is around 310 Volts during the whole simulation. The testing results show that the power output is still controlled within the correct range in case 2 when the irradiance to the PV and the wind speed is lower compared to that of case1; therefore, the control of the output power is proved to be successful.

4.2.3 Testing Case 3

To further test the control ability of the control system under various conditions, the microgrid system is tested in case 3, in which the wind speed is very low and the solar radiation is close to 0. The wind speed is 3.5 m/s (the cut-in wind speed is 3m/s) and the solar insolation is between 0 and 50 W/m^2. The results of the frequency and voltage of the microgrid are shown as below:

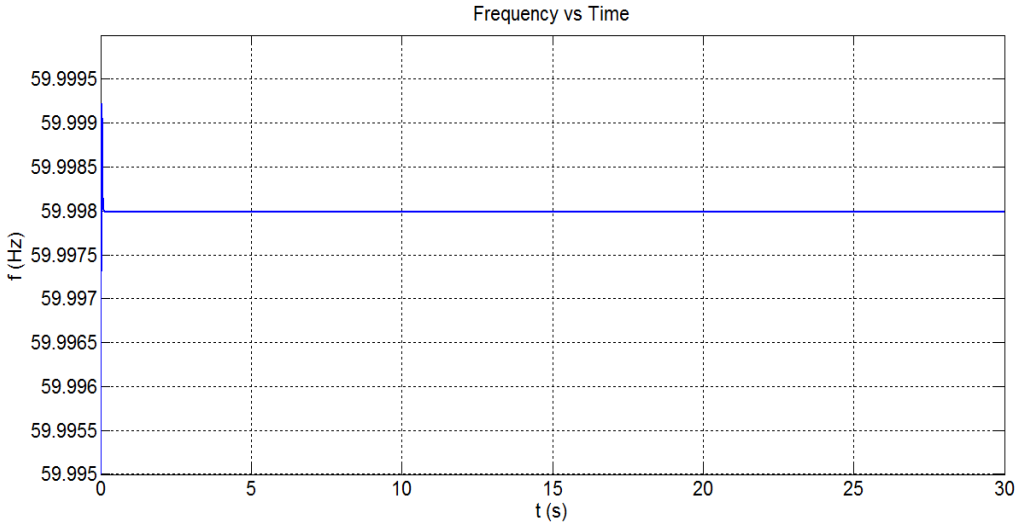

Figure 4.7 Frequency of Microgrid

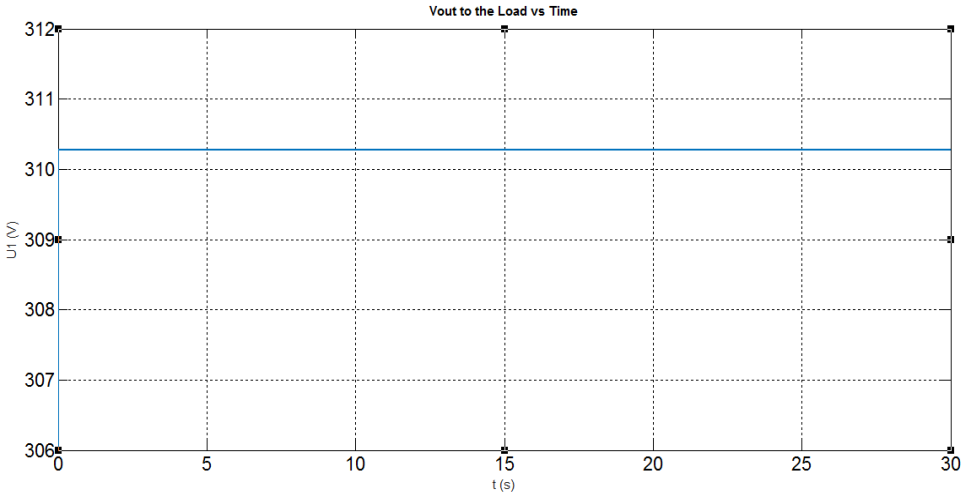

Figure 4.8 Voltage Output at the Load

Figure 4.7 shows that the frequency is controlled at 59.998Hz. From Figure 4.8, the voltage to the load bus is around 309 Volts during the whole simulation. Next is the power output from the PV system and the wind power system:

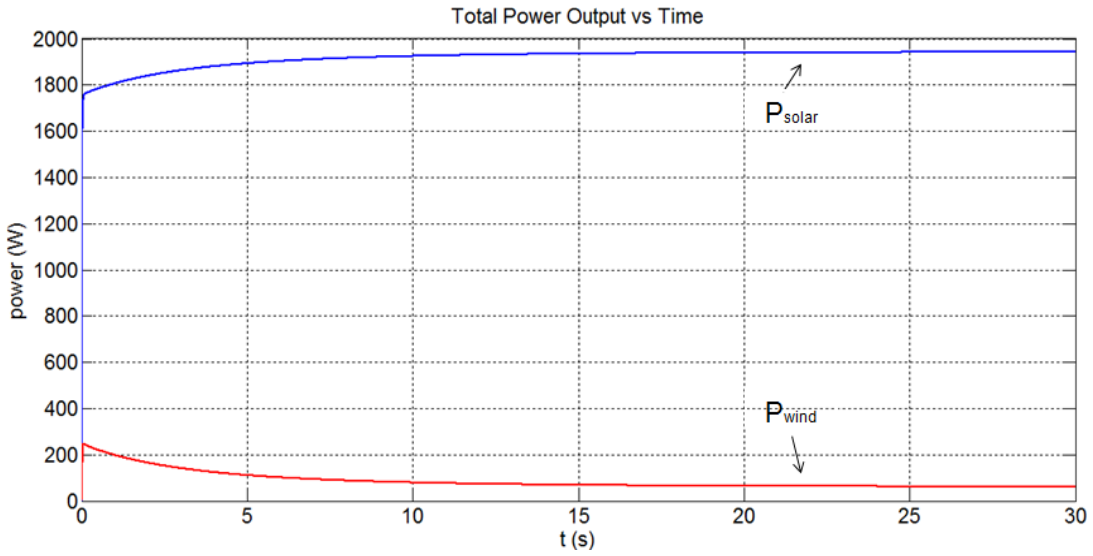

Figure 4.9 Total Power Output

The green line represents the wind power energy and the blue line blue line is the output of the PV system. By contrast, when both the irradiance to the solar panel and the wind speed are very low, the energy storage system takes its important role to support the power generation. The PV system takes the lead in the distributed generators. When wind speed decreases, the output power of the wind power system decreases and the battery energy storage system increases the power to balance the total power supply to the load. From Figure 4.9, the PV system and the BESS have the steady output around 1940 W after 12 seconds and the wind power system outputs 61.7 W; giving the total 2001.7 W to the load. The testing results show that when the solar radiation and wind speed are close

to 0, the Battery Energy Storage System (BESS) supplies power to the microgrid bus. Therefore, the successful control of the BESS is demonstrated.

4.3 Load 2

4.3.1 Test Case 4

Case 4 and 5 are the test cases with a different load than that of the case 1 to 3. Load 2 has the load of 3 kW. The phase to phase voltage and the frequency are the same as those of load 1. Case 4 is used to confirm that the pitch control system of the wind power plant functions well when the wind speed is higher than the upper limit bound (20 m/s). In this case, the irradiance to the solar panel increases in the morning and decreases after noon, the wind speed increases to more than 20 m/s at the peak and fluctuates throughout the day. The test results of the frequency and voltage are shown in the Figures 4.10 to 4.12 as below:

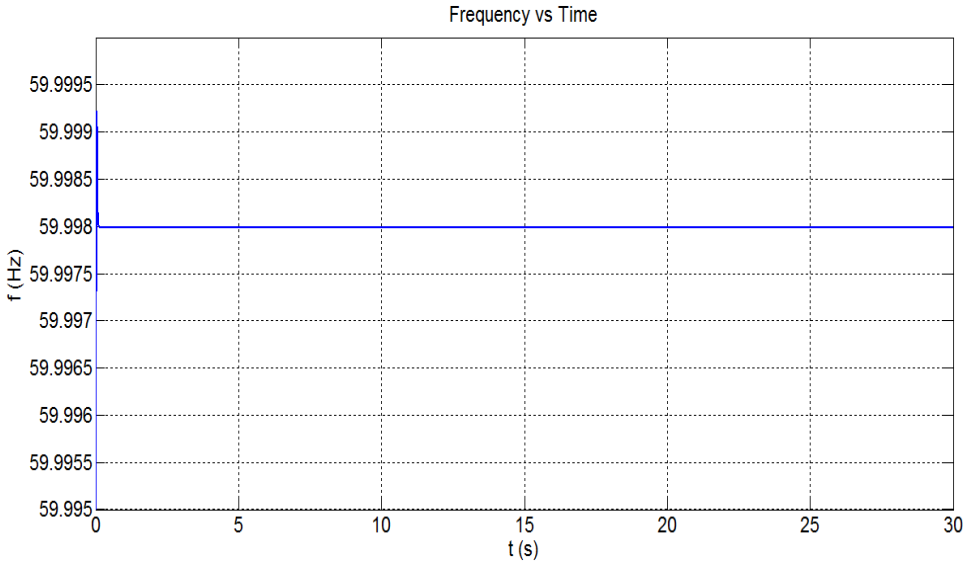

Figure 4.10 Frequency of Microgrid

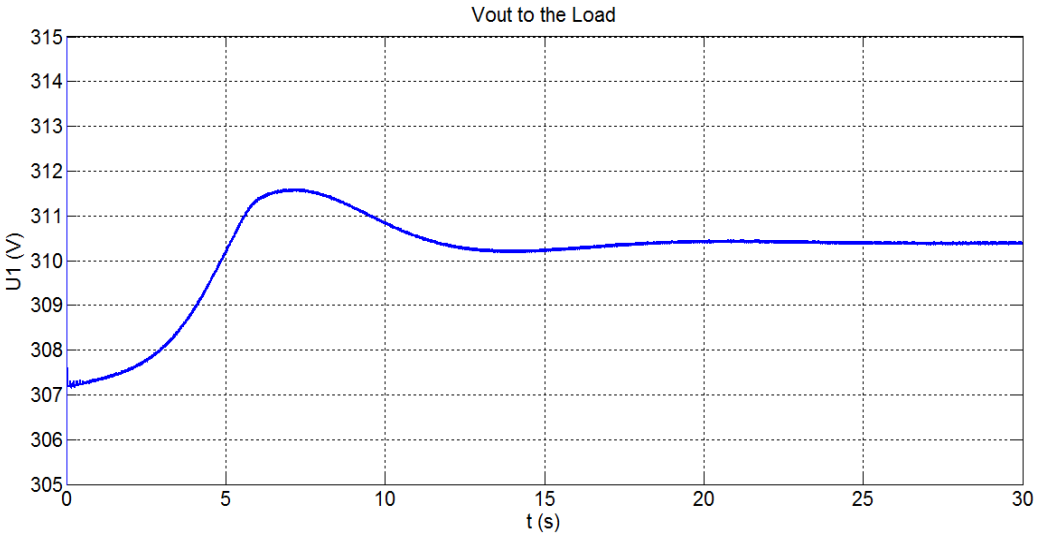

Figure 4.11 Voltage Output to the Load

From Figure 4.10 and Figure 4.11, the voltage to the load keeps at 308 V steadily after a few seconds and the frequency is controlled at 59.998 Hz while both the wind speed and the solar insolation fluctuate.

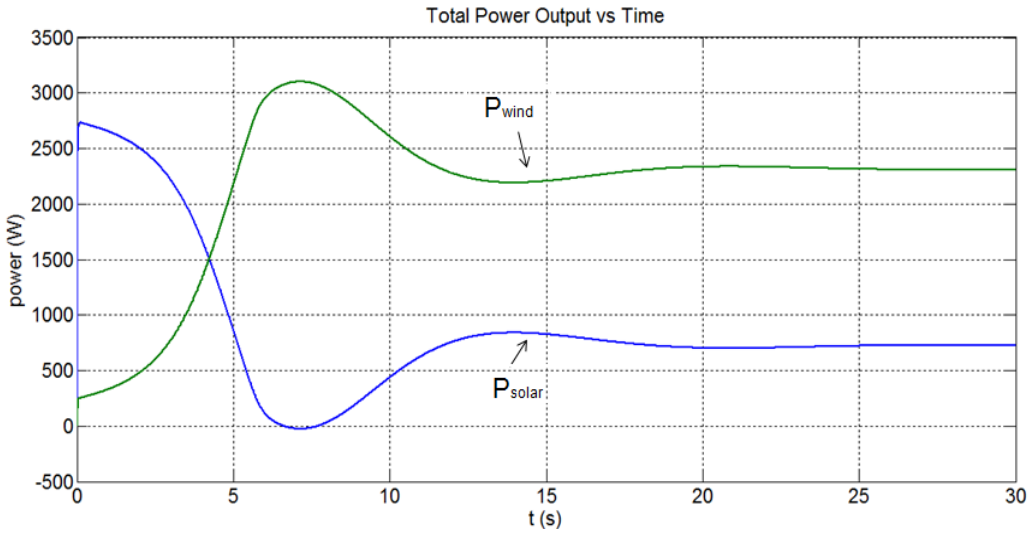

Figure 4.12 Total Power Output

In Figure 4.12, it is shown that both the output power of PV system and the wind power system fluctuates from 0 to 20 s. At first, the power output from the wind power system boosts up to more than 3 kW as the wind speed increases to more than 20 m/s. The PV system coordinates its output power based on the power output from the wind power system; for instance, when the wind power system outputs over 3 kW, the excess power goes to the PV system to charge the battery. The PV system outputs around 705 W while the wind power system outputs 2315 W, giving the total energy of approximately 3020 W to the load. In this case, the upper bound limit of the rotor speed is set to be 1.05 p.u. so the pitch controller adjusts the blade angle θ to control the rotor speed when the wind speed exceeds the rated value. Using equation (3.3), the output of the wind power system is controlled within the limit of $2000 * 1.05^3 = 2315\ W$. Thus, the simulation result has proved that the pitch controller has controlled the output of the wind power system within the limit range.

4.3.2 Testing Case 5

In the fifth case the load is 3 kW and the wind turbine has the wind speed at 9 m/s, the insolation still varies. The test results are shown in Figure 4.13 to Figure 4.15:

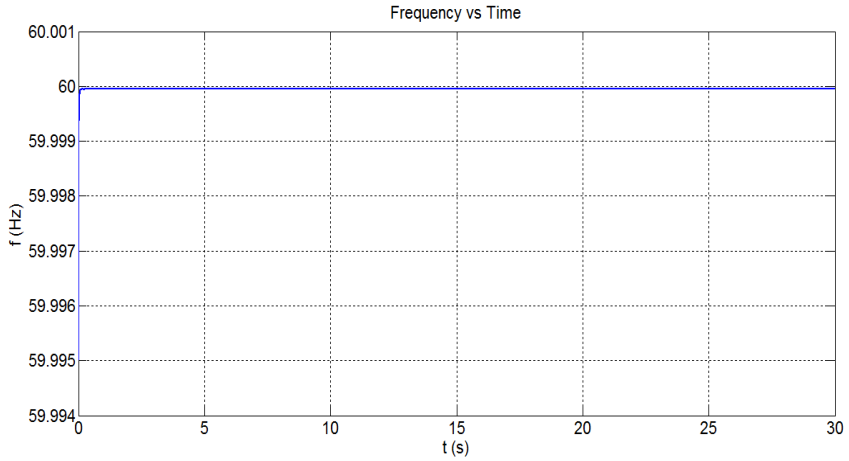

Figure 4.13 Frequency of Microgrid

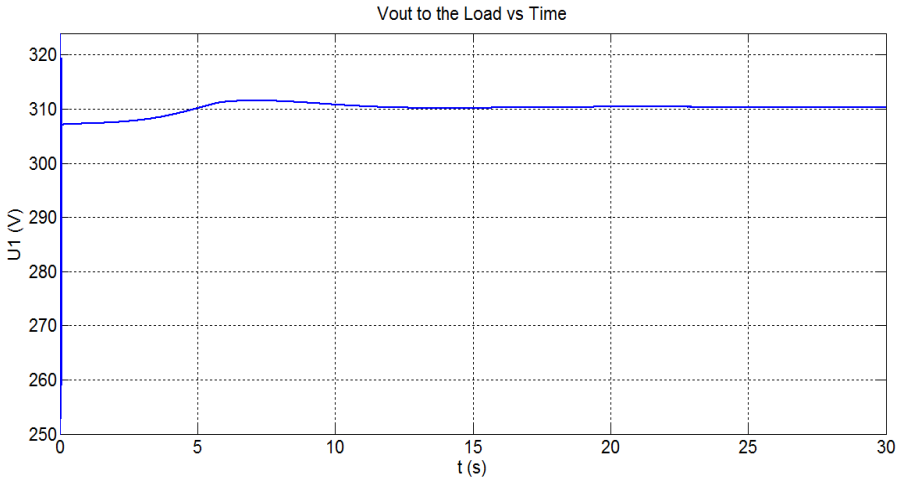

Figure 4.14 RMS Voltage Output at the Load

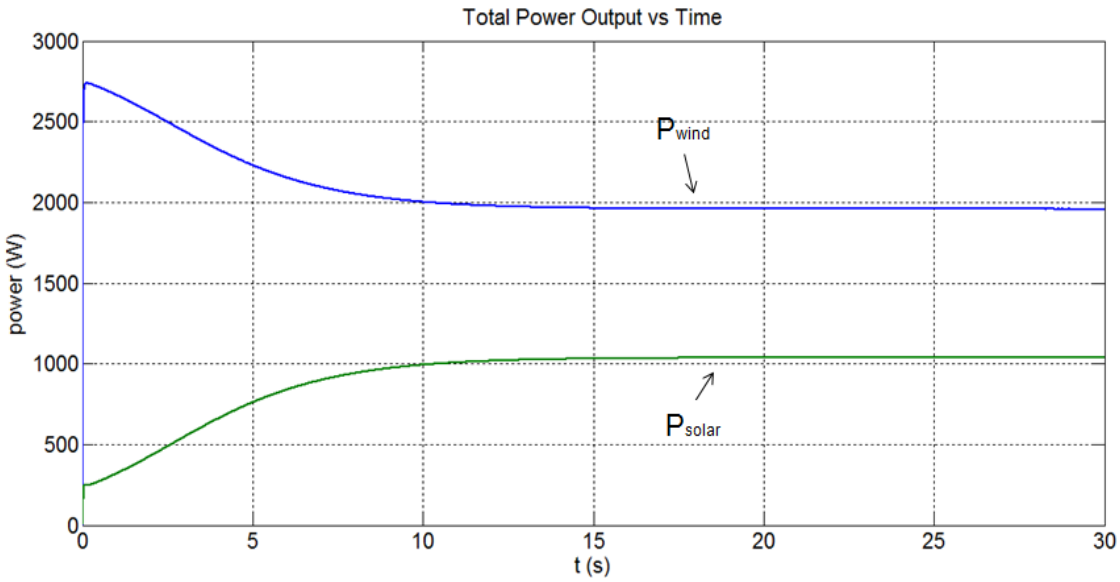

Figure 4.15 Total Output Power

As Figure 4.13 and 4.14 shows, when the wind speed is constant and the solar irradiance is low, both of the voltage and the frequency are controlled steadily and constantly.

In Figure 4.15, it is also shown that the output power of PV system and BESS gradually increases to 1035 W while the wind power system decreases to around 1965.1 W, giving the total energy of approximately 3000.1 W to the load. The output power control is proved to be successful in this case.

4.4 Discussion

By comparing and analyzing the results of the five case studies, the following conclusions can be obtained:

1 By comparing case 3 and case 5, the frequency and power are controlled successfully under different loads.

2 Case 3 and case 5 reflect the successful control capability of Battery Energy Storage System. The battery charges or discharges when the wind speed is too high or too low.

3 By comparing case 1 to case 5, the frequency and power are controlled successfully under different solar irradiance and wind speed.

4 Case 4 reflects the successful control of the pitch controller. When the wind speed exceeds the upper limit, the pitch controller changes the pitch angle in order to control the maximum output power of the wind power system.

Chapter Five: Conclusion and Future Work

5.1 Conclusion

Control of frequency and power are crucial problems for the microgrid. This thesis achieved the task of frequency stability control in the microgrid and it also demonstrated the ability of controlling the output power from the PV system and the wind power system. With respect to the expected contributions that are mentioned in chapter one, the thesis achieved the main contributions as follows:

1. Frequency stability is enhanced by using the droop controller integrated with virtual inertia, which is proved by comparing the frequency deviation under the control of the regular droop controller and that of the droop controller integrated with virtual inertia.

2. Steady control of the output power and the voltage in the microgrid is indicated by demonstrating the output power of the PV system and wind power system under various kinds of circumstances such as different amount of irradiance to the solar panel and different wind speed.

3. The successful control of the battery energy storage system (BESS) and the pitch controller to the output power is confirmed in case 3, case 4 and case 5.

4. The frequency, voltage and output power are controlled successfully under different loads.

5.2 Future Work

Though this thesis successfully tackles with the problem of control of frequency and power output, there are still some aspects for further research and improvement:

1. Proposed microgrid only has two distributed generators. More analysis and simulation could be done in order to expand the scale of microgrid.

2. Detailed microgrid mathematical model could be established in order to investigate the behavior of microgrid system. Optimized control algorithm coud be developed based on stability analysis of microgrid.

3. This microgrid is only designed and simulated through Matlab; in future research, other hardware and software such as RTDS (Real-time Digital Simulator) could be used to simulate the microgrid.

4. A protection relay could be added in the distribution system to protect the power distribution in the microgrid.

5. Distributed control architecture can be adopted in large-scale microgrid system in order to boost reliability and redundancy of microgrid control system.

References

[1] “Final Report on the August 14, 2003 Blackout in the United States and Canada, Causes and Recommendations”, April 2004

[2] "Power grids fail: Power restoration complete in Delhi & northeast, 50% in eastern region". *The Economic Times. 31 July 2012*. Retrieved 31 July 2012.

[3] Ernie Hayden. "Introduction to Microgrids" (PDF). Retrieved 20 June 2016

[4] Hatziargyriou, Nikos (2014). Microgrids Architectures and Control. John Wiley and Sons Ltd. p. 4. ISBN 978-1-118-72068-4.

[5] Ahmed M. Atallah, Almoataz Y. Abdelaziz, Raihan S. Jumaah, “Implementation of Perturb and Observe MPPT of PV System with Direct Control Method Using Buck and Buck-Boost Converters,” pp5, 2014

[6] Wenzhong Gao, “Energy Storage for Sustainable Microgrid ,” pp 80, 2015

[7] Bimal K. Bose. Global Energy Scenario and Impact of Power Electronics in 21st Century[J], IEEE Transactions on Industrial Electronics, 2013, 60(7): 2638-2651.

[8] Li Jun, Li F X, Li X Y, and etc. S-shaped droop control method with secondary frequency characteristics for inverters in microgrid [J]. IET Generation, Transmission & Distribution, 2016, 10(13): 3385-3392.

[9] Alipoor J, Miura Y, Ise T. Power system stabilization using virtual synchronous generator with alternating moment of inertia [J]. IEEE Journal of Emerging and Selected Topics in Power Electronics, 2015, 3(2):451-458.

[10] Ji Ping, Zhou Xiao Xin, Wu Shou Yuan. Review on Sustainable Development of Island Microgrid[C], The International Conference on Advanced Power System Automation and Protection, Beijing, China, 2011.

[11] Femia N, Petrone G, Spagnuolo G. Optimization of perturb and observe maximum power point trackingmethod [J]. IEEE Transactions on Power Electronics, 20(4): 963-973, 2005.

[12] Kasa N, Iida T, Chen L. Flyback inverter controlled by sensorless current MPPT for photovoltaic power system [J]. IEEE Transactions Industrial Electronics, 52(4): 1145–1152, 2005

[13] Jain S, Agarwal V. A new algorithm for rapid tracking of approximate maximum power point in photovoltaic systems [J]. IEEE Transactions on Power Electronics, 2(1): 16–19, 2004.

[14] S. Marinkov, B. Jager and M. Steinbuch, Extremum Seeking Control with Data-Based Disturbance Feedforward, in Proceedings of American Control Conference, 2014: 3627-3632.

[15] M. Krsti´c and H. Wang, Stability of Extremum Seeking Feedback for General Nonlinear Dynamic Systems, Automatica, 36(4): 595–601, 2000.

[16] Y. Tan, D. Nesic, and I. Mareels, On Non-local Stability Properties of Extremum Seeking Control, Automatica, 42(6): 889–903, 2006.

[17] A. Ghaffari, M. Krsti´c, S. Seshagiri, Power Optimization and Control in Wind Energy Conversion Systems using Extremum Seeking, IEEE Trans. on Control System Technology, 22(5): 1684-1695.

[18] T. Pan, Z. Ji, Z. Jiang, Maximum Power Point Tracking of Wind Energy Conversion Systems Based on Sliding Mode Extremum Seeking Control, in proceeding of Energy 2030 Conference, 2008: 1-5.

[19] M. Krsti´c, Performance Improvement and Limitations in Extremum Seeking Control, Systems & Control Letters, 39(5): 313–326, 2000.

[20] Y. Tan, D. Nesic, and I. Mareels, On Non-local Stability Properties of Extremum Seeking Control, Automatica, 42(6): 889–903, 2006.

[21] A. Ghaffari, M. Krsti´c, S. Seshagiri, Power Optimization and Control in Wind Energy Conversion Systems using Extremum Seeking, IEEE Trans. on Control System Technology, 22(5): 1684-1695.

[22] Alipoor J, Miura Y, Ise T. Power system stabilization using virtual synchronous generator with alternating moment of inertia [J]. IEEE Journal of Emerging and Selected Topics in Power Electronics, 2015, 3(2):451-458.

[23] Carrasco J M, Franquelo L G, Bialasiewicz J T and etc. Power-electronic systems for the grid integration of renewable energy sources: A survey [J], IEEE Transaction on Industrial Electronics, 2006, 53(4):1002-1016.

[24] Alaboudy A H K, Zeineldin H H, Kirtley J L. Microgrid stability characterization subsequent to fault-triggered islanded incidents [J], IEEE Transaction on Power Delivery, 2012, 27(2):658-669.

[25] Meegahapola L, Flynn D. Impact on transient and frequency stability for a power

system at very high wind penetration [C], IEEE Power Engineering Society General Meeting, 2010, pp. 1-8.

[26] Srivastava A K, Kumar A A, Schulz N N. Impact of distributed generators with energy storage devices on the electric grid [J], 2012, IEEE Systems Journal, 6(1):110-117.

[27] Wang D X, Wu H B. Application of virtual synchronous generator technology in microgrid [C], IEEE 8th International Power Electronics and Motion Control Conference(IPEMC), 2016, in process.

[28] L. Wu, D. Gao, Z. Cui, X. Kou, "A Novel Frequency Regulation Strategy with the Application of Energy Storage System for Large Scale Wind Power Integration," IEEE Annual Green Technology Conference, New Orleans, LA, 2015.

[29] J. Weber, D. Gao, X. Kou, J. Zhai, "Small Scale Grid Connected/Off-Grid Mobile Hybrid Integrated Renewable Energy System (HI-RES) for Rapid Recovery and Emergency Response," IEEE Annual Green Technology Conference, New Orleans, LA, 2015.

[30] Navid Goudarzi (June 2013). "A Review on the Development of the Wind Turbine Generators across the World". International Journal of Dynamics and Control. Springer. 1(2): 192–202. doi:10.1007/s40435-013-0016-y.

[31] Ahmed M. Atallah, Almoataz Y. Abdelaziz, Raihan S. Jumaah, "Implementation of Perturb and Observe MPPT of PV System with Direct Control Method Using Buck and Buck-Boost Converters," pp5, 2014

[32] Bin Wu, Yongqiang Lang, Navid Zargari, Samir Kouro "Power Conversion and Control of Wind Energy Systems," pp 42, 2011

[33] Wenzhong Gao, "Energy Storage for Sustainable Microgrid," pp 15, 2015

[34] http://www.mdpi.com/1996-1073/9/1/25/htm [j] Singh, K.J. et al., 2014. Artificial Neural Network Approach for More Accurate Solar Cell Electrical Circuit Model.*International Journal on Computational & Applications*, 4(3), pp.101–116.

[35] Sasaki, T., Ukyo, Y. and Novak, P. *Nat. Materials*, Advance Online Publication. *"Memory effect now also found in lithium-ion batteries". Retrieved 5 August 2015.*

[36] Marwali M N, Keyhani A. Control of distributed generation systems part Ⅰ: voltage and current control. IEEE Transaction on Power Electronics, 2004, 19(6):1541-1550.

[37] J. Kehler, “Considerations for load as a virtual generator for grid security,” in Proc. IEEE Power Eng. Soc. Gen. Meeting, Jul. 2003, vol. 4, pp. 2289–2292.

[38] H. P. Beck and R. Hesse, “Virtual synchronous machine,” in Proc. 9th Int. Elect. Power Quality Utilisation, Oct. 2007, pp. 1–6.

[39] J. Driesen and K. Visscher, “Virtual synchronous generators,” in Proc. IEEE Power Energy Soc. Gen.Meeting—Convers. Del. Elect. Energy 21st Century, Jul. 2008, pp. 1–3.

[40] S. De Haan, R. VanWesenbeeck, and K. Visscher. (2008, Oct.) VSG control algorithms: present ideas. [Online]. Available: http://www.vsync.eu. Project VSYNC.

[41] K. Visscher and S. De Haan, “Virtual synchronous machines (VSGs) for frequency stabilisation in future grids with a significant share of decentralized generation,” in Proc. IET-CIRED Semin. SmartGrids Distrib., Jun. 2008, pp. 1–4.

[42] Q. C. Zhong and G.Weiss, “Static synchronous generators for distributed generation and renewable energy,” in Proc. IEEE Power Energy Soc.Power Syst. Conf. Expo., Mar. 2009, pp. 1–6.

[43] M. Van Wesenbeeck, S. de Haan, P. Varela, and K. Visscher, “Grid tied converter with virtual kinetic storage,” in *IEEE Bucharest PowerTech*, Jul. 2009, pp. 1–7.

[44] Q. C. Zhong and G. Weiss, “Synchronverters: Inverters that mimic synchronous generators,” *IEEE Trans. Ind. Electron.*, vol. 58, no. 4, pp. 1259–1267, Apr. 2011.

[45] H. Bevrani, T. Ise, and Y. Miura, “Virtual synchronous generators: A survey and new perspectives,” *Int. J. Elect. Power Energy Syst.*, vol. 54, no. 1, pp. 244–254, Jan. 2014.

[46] http://www.openelectrical.org/wiki/index.php?title=Droop_Control

[47] Qing-Chang Zhong, George Weiss “Synchronverters: Inverters That Mimic Synchronous Generators,” IEEE Transactions on Industrial Electronics, Vol.58, NO.4, April 2011

[48] A Wind Energy Pioneer: Charles F. Brush. Danish Wind Industry Association. Retrieved 2008-12-28.

[49] Xiao Wang, Wenzhong Gao, Weihang Yan, “Evaluation of the Inertia Response of Variable-Speed Wind Turbines”

[50] Ross Vennell, Tuning tidal turbines in-concert to maximise farm efficiency, Journal of Fluid Mechanics 671 (2011) 587-604.doi:10.1017/S0022112010006191

[51] Xiao Wang, Wenzhong Gao, Weihang Yan, “Initial Response of Wind Power Plants: A Comparison of Frequency-based Inertial Control and Stepwise Inertia Control”

[52] "Renewables 2011: Global Status Report". REN21. 2011. p. 22